bioRxiv preprint doi: https://doi.org/10.1101/2021.11.15.468604; this version posted November 15, 2021. The copyright holder for this preprint (which was not certified by peer review) is the author/funder, who has granted bioRxiv a license to display the preprint in perpetuity. It is made available under aCC-BY 4.0 International license.

Molecular dynamics simulations reveal the selectivity mechanism of structurally similar agonists to TLR7 and TLR8

Xiaoyu Wang[1], Yu Chen[1], Steven Zhang[2], Jinxia Nancy Deng[3]*

1 Computational Chemistry Department, Shanghai ChemPartner Co., Ltd., 576 Libing Road, Shanghai 201203, China

2 Chemistry Department, Shanghai ChemPartner Co., Ltd., 576 Libing Road, Shanghai 201203, China

3* corresponding author, Computational Chemistry Department, ChemPartner, 280 Utah Ave, South San Francisco, CA, 94080

Abstract

TLR7 and TLR8 are key members of the Toll-like receptor family, playing crucial roles in the signaling pathways of innate immunity, and thus become attractive therapeutic targets of many diseases including infections and cancer. Although TLR7 and TLR8 show a highly degree of sequence homology, their biological response to small molecule binding is very different. Aiming to understand the mechanism of selective profiles of small molecule modulators against TLR7 and TLR8, we carried out molecular dynamic simulations on three imidazoquinoline derivatives bound to the receptors separately. They are Resiquimod (R), Hybrid-2 (H), and Gardiquimod (G), selective agonists of TLR7 and TLR8. Our MD trajectories indicated that in the complex of TLR7-R and TLR7-G, the two chains forming the TLR7 dimer tended to remain "open" conformation, while the rest systems maintained in the closed format. The agonists R, H, and G developed conformational deviation mainly on the aliphatic tail. Furthermore, we attempted to quantify the selectivity between TLR7 and TLR8 by binding free energies via MM-GBSA method. It showed that the three selected modulators were more favorable for TLR7 than

bioRxiv preprint doi: https://doi.org/10.1101/2021.11.15.468604; this version posted November 15, 2021. The copyright holder for this preprint (which was not certified by peer review) is the author/funder, who has granted bioRxiv a license to display the preprint in perpetuity. It is made available under aCC-BY 4.0 International license.

TLR8, and the ranking from the strongest to the weakest was H, R and G, aligning well with experiment data. In the TLR7, the flexible and hydrophobic aliphatic side chain of H has stronger van der Waals interactions with Val381 and Phe351 but only pick up interaction with one amino acid residue i.e. Tyr353 of TLR8. Unsurprisingly, the positively charged side chain of G has less favor interaction with Ile585 of TLR7 and Val573 of TLR8 explaining G is weak agonist in both TLR7 and TLR8. All three imidazoquinolines can form stable hydrogen bonds with Asp555 of TLR7 and the corresponding Asp543 of TLR8. In brief, the set of total 400ns MD studies sheds light on the potential selective mechanisms of agonists towards TLR7 and TLR8, indicating the van der Waals interaction as the driving force for the agonists binding, thus provides us insights for more potent and selective modulators to cooperate with the hydrophobic nature of the binding pocket.

Key words: Toll-like receptor, TLR7 TLR8 selectivity, TLR7 agonist, TLR8 agonist, Resiquimod, Hybrid-2, Gardiquimod, molecular dynamics, MM-GBSA, binding free energy, TLR modulator

1. Introduction

Toll-like receptors (TLRs) are a large family of proteins, playing an important part in innate immune system, that recognize structurally conserved molecules, such as single-stranded (ss) or double-stranded (ds) RNAs or DNAs, lipoproteins and lipopolysaccharides derived from microbes and then activate immune cell responses [1]. A typical TLR is a single-spanning receptor consisting of three domains: an extracellular domain (ECD) with variable number of leucine-rich repeat sequences (LRRs) for the recognition of pathogen-associated molecular patterns (PAMPs), a transmembrane domain (TMD), and an intracellular Toll-interleukin 1 receptor (TIR) domain

bioRxiv preprint doi: https://doi.org/10.1101/2021.11.15.468604; this version posted November 15, 2021. The copyright holder for this preprint (which was not certified by peer review) is the author/funder, who has granted bioRxiv a license to display the preprint in perpetuity. It is made available under aCC-BY 4.0 International license.

initiating downstream signaling [2]. Until now, thirteen TLRs have been identified, and among which, TLR3, TLR7, TLR8, and TLR9 are located in intracellular membranes because they are sensors of nucleic acids. Specifically, TLR3 recognizes viral dsRNA, and TLR9 senses unmethylated cytosine phosphate guanosine (CpG) containing DNA, whereas TLR7 and TLR8 both locate in endosomal membrane and function as viral ssRNA sensors [3].

Many studies have revealed that the expression levels of TLR7 and TLR8 are altered in some autoimmune diseases, such as arthritis, cancers [4-8], or in antiviral regimes, including corona virus prevention and HIV [9]. Thus, novel drug design and development against TLR7 or TLR8 became very attractive.

In the last few years, many TLR7 or TLR8 agonists with different scaffolds have been developed. These agonists leading to the induction of certain IFNs, cytokines and chemokines can be applied to the treatment of some diseases and good adjutants of vaccines [10-12].

The drug development of TLR modulators requires a solid understanding of TLR7 and TLR8 activity regulation. TLR7 and TLR8, sharing high degree of sequence homology and three dimensional structure similarity, are both known to serve as endosomal pattern recognition receptors (PRRs) for a number of RNA viruses, such as HIV, coronaviruses, influenza etc [9,13-16]. However, there still exist many distribution and function differences between these two closely related proteins. TLR7 is mainly expressed in plasmacytoid dendritic cells (pDC) and B cells [17-19]. But TLR8 is mainly expressed in myeloid dendritic cells (mDC), monocytes, macrophages and neutrophils [17,20,21]. TLR7 recognizes guanosine and its derivatives [22]while TLR8 serves as a uridine receptor [23]. Moreover, interferons induced by pDC are the major production of TLR7 signaling [24], whereas TLR8 signaling mainly results in NF-kB pathway activation and subsequent proinflammatory cytokines and chemokines expression [25]. To understand how TLR7 and TLR8 can recognize different ligands, and as consequence to activate different signaling

bioRxiv preprint doi: https://doi.org/10.1101/2021.11.15.468604; this version posted November 15, 2021. The copyright holder for this preprint (which was not certified by peer review) is the author/funder, who has granted bioRxiv a license to display the preprint in perpetuity. It is made available under aCC-BY 4.0 International license.

pathways, we design computational simulations to investigate the selective mechanism of small molecule agonists between TLR7 and TLR8.

Molecular dynamics (MD) simulation is a very established computational technique to understand the protein structure-function relationship and guide the drug design. Since the first case of MD on Bovine pancreatic trypsin inhibitor, in the late 70s [26], MD and its applications have been extended successfully in many areas. Especially in recent years, benefit from the development of modern graphics processing units (GPUs) hardware and progress of force fields, MD simulation has made huge impact to life science research. Some great progress can be exemplified by understanding the dynamics of protein conformation which is hardly available by current experimental techniques, such as the folding and aggregation of amyloid-related proteins [27-29], and conformational transition caused by mutations, temperature and PH values [30-34]. MD simulation has also play an important role in characterizing receptor-ligand interaction (protein-protein, protein-DNA/RNA, protein-small molecule) [35-37]. Besides, it helps to reveal the novel binding sites which have not been captured by NMR and X-ray crystallographic analysis. For example, cryptic binding sites in HIV-1 integrase [38], cruzain [39] and Ras [40] and five allosteric sites of human β1(β1AR) and β2 (β2AR) adrenergic receptor [41] were served as new drug targets. In addition, MD simulation provides multiple typical conformations which can be used for virtual screening to obtain more reasonable ligand binding modes [42-47]. And it can optimize the position between protein and ligand with estimation of the average binding free energy, providing the guidance of structural based drug design [48-50]. Up to now, MD simulations have been successfully applied to many large systems, such as the complete HIV1 capsid with 64 million atoms up to 100ns [51], satellite tobacco mosaic capsid of 1 million atoms up to 50ns [52], southern bean mosaic capsid of 4.5 million atoms up to 100ns [53], and ribosome of 2.64 million atoms [54]. For some systems, MD simulation has been instrumental on understanding the protein folding and function regulation with a simulation time of 10-100us [55-57].

bioRxiv preprint doi: https://doi.org/10.1101/2021.11.15.468604; this version posted November 15, 2021. The copyright holder for this preprint (which was not certified by peer review) is the author/funder, who has granted bioRxiv a license to display the preprint in perpetuity. It is made available under aCC-BY 4.0 International license.

Because of the above mentioned success, not surprisingly, some MD simulations were carried out on TLRs, such as the stability of vaccine and TLRs [58,59], TLRs model [60,61] and effect of mutations on TLRs dimer [62]. MD simulation was applied to equilibrate homology model of TLR7, proposing the appropriate TLR7 dimer structure and studying the binding site and residues significant for dimerization [63]. And it was used to explain the difference of interaction mode between agonists and antagonists (including imidazoquinoline and adenine derivatives) against TLR7 [64]. Targeted molecular dynamics (TMD) was employed to study the conformational transition of TLR8 dimerization, illuminating the internal mechanism of relatively aggregate movement of two TLR8 chains [65]. These research results have inspired our research ideas.

Some imidazoquinoline derivatives (Fig 1), i.e. Resiquimod (R) [66,67], Hybrid-2 (H) [68] and Gardiquimod (G) [69] are agonists of TLR7 and TLR8. They carry the common core of the same parent nucleus, whereas the side chain is oxygen, carbon, nitrogen atom, respectively. However, this one-atom difference in the chemical structure results in magnitude difference in their biological activity on TLR7 and TLR8. In general, they are more potent on TLR7 than those on TLR8 (Table 1). These two facts aroused our interest in investigating the agonist selectivity for TLR7 and TLR8 by MD simulations.

In this work, first, eight systems were built, and they are TLR7 (apo), TLR7-R, TLR7-H, TLR7-G, TLR8 (apo), TLR8-R, TLR8-H, and TLR8-G, respectively. Second, 50ns MD simulations of each of the eight systems were performed. Subsequently, the binding free energy of each ligand with TLR7, and TLR8 was calculated respectively using the MM-GBSA method. The interactions between the three agonists with TLR7 and TLR8 were analyzed to explain the intrinsic mechanism of the selectivity mechanism of the three agonists at the atomic level.

Fig 1. The chemical structures of the three agonists: Resiquimod (R), Hybrid-2 (H) and Gardiquimod (G).

bioRxiv preprint doi: https://doi.org/10.1101/2021.11.15.468604; this version posted November 15, 2021. The copyright holder for this preprint (which was not certified by peer review) is the author/funder, who has granted bioRxiv a license to display the preprint in perpetuity. It is made available under aCC-BY 4.0 International license.

2. Materials and methods

2.1 Research Systems

To investigate the selectivity of R, H and G with TLR7 and TLR8, respectively, the eight systems for the study are TLR7 (apo), TLR7-R, TLR7-H, TLR7-G, TLR8 (apo), TLR8-R, TLR8-H and TLR8-G. The crystal structures obtained from the Protein Data Bank (PDB) were used as the templates, and the codes are 5GMH (TLR7-R) [22], 5ZSG (TLR7-G), 3W3N (TLR8-R) [70], 4R6A (TLR8-H). The apo TLR7 was modeled from the x-ray complex of TLR7-R (5GMH) by removing the ligand and same to the apo TLR8 from TLR8-R (3W3N). The TLR7-H system was modeled based on coordinates of TLR7-R by replacing the oxygen to carbon atom. Similarly, the TLR8-G system was modeled by replacing the oxygen atom on alkyl chain in TLR8-R with a nitrogen atom. The crystal structures were connected for the missing residues via SWISS-MODEL server [71]. The modeled structures were aligned to their crystal structures and were retained with corresponding ligand. The sequence fragment between amino acid residue 434-458 was removed to align with the biological understanding that those motifs in both TLR7 and TLR8 are cleaved prior to the activation process [70,72]. In fact, these residues are also missing in 3W3N and 4R6A crystal structures. With reference on the recent research that human TLR7 and TLR8 proteins are in acidic endolysosom (pH is around 5) [73,74], the protonation states of agonists were predicted by Maestro (from Schrödinger V.2019-4) [75] at the pH value of 5(±0.5). The nitrogen atoms on quinoline ring in all complex systems and nitrogen atoms on alkyl chain in TLR7-G system and TLR8-G system are protonated.

bioRxiv preprint doi: https://doi.org/10.1101/2021.11.15.468604; this version posted November 15, 2021. The copyright holder for this preprint (which was not certified by peer review) is the author/funder, who has granted bioRxiv a license to display the preprint in perpetuity. It is made available under aCC-BY 4.0 International license.

2.2 Molecular dynamic simulation

All MD simulations were carried out in the isothermal isobaric (NPT) ensemble with periodic boundary condition by the program GROMACS (version 2020.4-GPU package) [76]. The AMBER ff99SB force filed [77] was applied to model proteins and the general amber force filed (GAFF) [78] was assigned to model the small molecule agonists. Each system was placed in a rectangular box of TIP3P explicit water molecules with a minimum distance to the water box wall of 9 Å [79], and counterions (Cl^{-1}) were added to neutralize the system. Each simulation system was first subjected to energy minimization using the steepest descents algorithm. Then, a simulation was carried out to heat the system to 300K with the protein fixed using a harmonic restraint. The temperature was kept close to 300K by V-rescale thermostat [80] and the pressure was kept at 1 bar using the Parrinello-Rahman pressure coupling scheme [81]. The LINCS method [82] was used to restrain bond lengths that including hydrogen atoms, allowing an integration step of 2 fs. Finally, based on the relaxed system, the long-time simulation so called the production phase was performed without any constraints for 50ns.

2.3 Binding free energy calculation

The MM-GBSA binding free energy calculations between the protein and agonist were using MMPBSA.py module in AmberTools20 package. The binding free energy ($\Delta G_{binding}$) between a receptor and a ligand and can be estimated using Equation 1:

$$\Delta G_{binding} = \Delta E_{MM} + \Delta G_{solv} - T\Delta S \quad (1)$$

ΔE_{MM} : the gas phase energy consisting of electrostatic (ΔE_{elec}) and van der Waals (ΔE_{vdW}) terms. ΔG_{solv} : solvation energy including both the polar solvation energy, ΔG_{polar} and the nonpolar solvation component, ΔG_{surf}. The ΔG_{polar} in above equation is calculated by the GB model [83] and ΔG_{suf} is estimated by the solvent accessible surface area (SASA). $\Delta G_{binding}$: the relative binding free energy. $T\Delta S$: the entropy term. It is usually suitable for systems with large conformational

bioRxiv preprint doi: https://doi.org/10.1101/2021.11.15.468604; this version posted November 15, 2021. The copyright holder for this preprint (which was not certified by peer review) is the author/funder, who has granted bioRxiv a license to display the preprint in perpetuity. It is made available under aCC-BY 4.0 International license.

168 changes, thus was ignored in our simulations, aligning with other previous computational studies
169 [84,85].

170

171 **3. Result and Discussion**

172 **3.1 Characterization of conformational changes in the systems**

173 The conformational changes of the eight simulated systems, ie TLR7 (apo), TLR7-R, TLR7-
174 H, TLR7-G, TLR8 (apo), TLR8-R, TLR8-H, TLR8-G systems were first analyzed in terms of the
175 root mean square deviation (RMSD) of protein backbone in each system (Fig 2). The RMSD
176 values of TLR7 (Fig 2A) in the three complex systems change from the initial value (0 ns) to a
177 scope of 2.5-4.0 Å, maintaining in this scope after 30 ns. Among these three, TLR7-G system,
178 represented by the green line has the largest RMSD value close to 4 Å, and therefore the largest
179 deviation comparing with the rest agonists. Throughout most of the simulation, TLR7-R and
180 TLR7-H systems have similar RMSD plots to one another.

181 The RMSD values of TLR8 (Fig 2B) in the three complex systems change from the initial
182 value (0 ns) to a scope of 2.0-3.0 Å and then also maintain in this scope after 30 ns. Among these
183 three, TLR8-R, TLR8-H and TLR8-G systems have the similar RMSD plot during most of the
184 simulation time. These reveal the larger conformational change of complex systems presented on
185 TLR7 compared to that of TLR8. It can be observed that the RMSD value in the TLR8 (apo)
186 system is slightly higher than those of the TLR8 complex systems after 30 ns, which indicates
187 that the TLR8 is more flexible in the presence of agonist. The RMSD value in the TLR7 (apo)
188 system is slightly lower than those of the TLR7 complex system after 30 ns, which indicates that
189 the TLR7 is less flexible in the absence of agonist.

190

bioRxiv preprint doi: https://doi.org/10.1101/2021.11.15.468604; this version posted November 15, 2021. The copyright holder for this preprint (which was not certified by peer review) is the author/funder, who has granted bioRxiv a license to display the preprint in perpetuity. It is made available under aCC-BY 4.0 International license.

Fig 2. The overall RMSD values of TLR7 and TLR8 with and without the agonists. (A) TLR7 (apo) system, TLR7-R system, TLR7-H system and TLR7-G system. (B) TLR8 (apo) system, TLR8-R system, TLR8-H system and TLR8-G system.

In addition, the trajectories displayed in Fig 3 using VMD software [86] to observe conformation changes show that the two chains (i.e. chain A and chain B) in TLR7 of the TLR7-R and TLR7-G systems were gradually open measured by the distances between the anchor points in the first 30 ns, but the TLR7-H system maintained the closed conformation state. In order to describe the closed and open conformational changes, the centroid of Arg784 backbone atoms in chain A and chain B of TLR7 were defined as anchor points to calculate the time-dependent distance between two chains (Fig 3A). In the same way, the centroid of Pro773, the corresponding counterpart in TLR8 of Arg784 in TLR7, backbone atoms in chain A and chain B of TLR8 were chosen as anchor points (Fig 3B). These two pairs of amino acid residues were chosen as anchor points because they are located on the central axis and closest to the bottom of the two chains. In complex systems, the distance between the two Arg784 are both gradually increased in TLR7-R and TLR7-G systems, though the range in TLR7-G is greater than TLR7-R (Fig 3C). The distance changes in TLR7-H, TLR8-R, TLR8-H and TLR8-G systems are not evident (Fig 3C and Fig 3D). In apo systems, the distance changes in TLR7 and TLR8 systems are also not evident (Fig 3C and Fig 3D).

Fig 3. The distance changes of chain A and chain B for TLR7 and TLR8. (A) The Arg784 of each chain is defined as anchor point on TLR7. (B) The Pro773, counterpart of Arg784 of TLR7, of each chain is defined as anchor point on TLR8. (C) The time dependent distance between chainA-Arg784 and chainB-Arg784. (D) The time dependent distance between chainA-Pro773 and chainB-Pro773.

bioRxiv preprint doi: https://doi.org/10.1101/2021.11.15.468604; this version posted November 15, 2021. The copyright holder for this preprint (which was not certified by peer review) is the author/funder, who has granted bioRxiv a license to display the preprint in perpetuity. It is made available under aCC-BY 4.0 International license.

3.2 Conformational changes of pocket residues and agonists

The amino acid residues within 6 Å of the agonists were defined as the pocket residues in this work. The RMSD values of backbone atoms (Fig 4A and Fig 4B) and heavy atoms (Fig 4C and Fig 4D) of pocket residues were calculated respectively. The RMSD values of backbone atoms in the four TLR7 systems change from the initial value (0 ns) to a scope of 1.0-2.0 Å, and 1.5-2.5 Å for heavy atoms, maintaining in this scope after 30 ns. In these four systems, the RMSD values of pockets in the TLR7 (apo) and TLR7-H systems are the lowest and the RMSD values of residues in TLR7-R and TLR7-G systems are nearly the same. It reveals that the pocket of TLR7 is less flexible in the TLR7 and TLR7-H systems. The RMSD values of backbone atoms and heavy atoms in the four TLR8 systems change from the initial value (0 ns) to a scope of 1.2-2.5 Å and 1.5-3.0 Å, maintaining in this scope after 30 ns. In these four systems, the RMSD value of pocket residues in the TLR8-H system is the lowest of the four, while the RMSD values of pocket residues in the TLR8, TLR8-R and TLR8-G systems are nearly the same. It reveals that the pocket of TLR8 is less flexible in the TLR8-H system compared to TLR8 (apo), TLR8-R and TLR8-G systems. The above analysis suggests that the pockets residues of TLR8 were more flexible than that of TLR7, though the overall conformation change of TLR8 is smaller than that of TLR7 (Fig 3).

Fig 4. The RMSD values of the pocket residues in each system defined by 6 Å away from the agonists. (A) RMSD of backbone atoms of TLR7 pocket. (B) RMSD of backbone atoms of TLR8 pocket. (C) RMSD of heavy atoms of TLR7 pocket. (D) RMSD of heavy atoms of TLR8 pocket.

On the other hand of the trajectory analysis, we also examine the conformational change of agonists. The heavy atom RMSD of agonists was calculated in the six TLR-agonist systems (Fig

bioRxiv preprint doi: https://doi.org/10.1101/2021.11.15.468604; this version posted November 15, 2021. The copyright holder for this preprint (which was not certified by peer review) is the author/funder, who has granted bioRxiv a license to display the preprint in perpetuity. It is made available under aCC-BY 4.0 International license.

5B and Fig 5E) with respect to the initial conformation. The RMSD of agonists in TLR7 and TLR8 complex systems increase from the initial value (0 ns) to a scope of 1.0-3.0 Å and all reach maintain in this scope after 30 ns. However, three agonists show significant differences in fluctuation range. The fluctuations are largest inTLR7-G and TLR8-G, and the fluctuations are smallest in TLR7-R and TLR8-R. The conformations of the three agonists were superimposed on the imidazoquinoline ring, and the initial frame (0 ns) and a frame near the late stage of the simulation (40 ns) were selected for comparison. In the initial frame, all atoms of the agonists of TLR7 (Fig 5A) and TLR8 (Fig 5D) complex systems are superimposed nicely. The alignment at t = 40 ns of snapshot was chose to represent every conformation in the simulation 30-50 ns, the side chain orientations of the ligands in TLR7 (Fig 5C) and this in TLR8 (Fig 5F) are apparently different.

Fig 5. The conformational change of the agonists. Schematic diagram of three TLR7 agonists superimposed on the imidazoquinoline ring at 0 ns (A) and 40 ns (C). Schematic diagram of three TLR8 agonists superimposed on the imidazoquinoline ring at 0 ns (D) and 40 ns (F). RMSD values of agonists in TLR7 complex systems (B) and TLR8 complex systems (E).

3.3 MM-GBSA binding free energy

Aiming to quantify the selectivity profile between the agonists and TLR7 and TLR8, the last 20 ns of simulation data was applied for MM-GBSA binding free energy analysis. The predicted binding free energies of R, H and G binding to TLR7 or TLR8 are summarized in Table 1. The binding free energies of R, H and G binding to TLR7 are -44.21 kcal/mol, -50.50 kcal/mol and -33.65 kcal/mol, respectively. The binding free energies of R, H and G binding to TLR8 are -39.55 kcal/mol, -42.09 kcal/mol and -20.99 kcal/mol. The results indicate that H shows the strongest binding affinity, and G is the weakest. Additionally, the binding affinity of each of the agonists

bioRxiv preprint doi: https://doi.org/10.1101/2021.11.15.468604; this version posted November 15, 2021. The copyright holder for this preprint (which was not certified by peer review) is the author/funder, who has granted bioRxiv a license to display the preprint in perpetuity. It is made available under aCC-BY 4.0 International license.

with TLR7 is stronger than that of TLR8, consistent with previously published experimental data of R, H and G [68,87-89].

To better understand the binding profile, key binding contributors were also analyzed and summarized in Table 2 for TLR7, and in Table 3 for TLR8. Specifically, van der Waals interaction makes a major contribution to binding free energy. In TLR7-H and TLR7-R systems, there are stronger van der Waals interactions compared to the TLR7-G system. In TLR8-H and TLR8-R systems, there are also stronger van der Waals interactions compared to the TLR8-G system. The van der Waals interactions of TLR7 complex systems are overall stronger than that of TLR8 complex systems. The total contribution from the electrostatic interaction and polar solvation energy is unfavorable to binding. TLR7-H and TLR8-H systems have the strongest binding affinity as compared to that of corresponding complex systems, because of lower van der Waals energies and contribution from the electrostatic interaction and polar solvation energy. The above indicates that the pockets of TLR7 and TLR8 are hydrophobic pockets. Furthermore, the energy decomposition values of binding free energy were calculated to get insight into the binding mode of the agonists with TLR7 and TLR8. Items that contributed less than -1.0 kcal/mol to the binding free energy are listed in Table S1-S6. In Fig S1 and Fig S2, the values of these main residues are displayed in a bar graph.

Table 1. Predicted binding free energies and experimental EC50 values of R, H and G

Compound	TLR7		TLR8	
	Predicted binding free energy (kcal/mol) [a]	**EC50 (nM)**	**Predicted binding free energy (kcal/mol) [a]**	**EC50 (nM)**
R	-44.21	1400[87]	-39.55	6400[87]
H	-50.50	2.5[68]	-42.09	19[68]
G	-33.65	2000[88]	-20.99	No activation

bioRxiv preprint doi: https://doi.org/10.1101/2021.11.15.468604; this version posted November 15, 2021. The copyright holder for this preprint (which was not certified by peer review) is the author/funder, who has granted bioRxiv a license to display the preprint in perpetuity. It is made available under aCC-BY 4.0 International license.

of NF-κB[89]

[a] The predicted binding free energies were obtained based on 30-50 ns MD simulation trajectory. A total of 201 snapshots evenly extracted from the 30-50 ns MD trajectory of each complex system were used for MM-GBSA calculations.

Table 2. Results of MM-GBSA method of R, H and G to TLR7[b]

Item	TLR7-H	TLR7-R	TLR7-G
van der Waals	-45.72	-45.24	-34.60
Electrostatic	398.07	393.98	788.50
Polar solvation	-396.95	-387.33	-783.04
Non-polar Solv.	-5.90	-5.63	-4.52
$\Delta E_{pol,ele}$	1.12	6.65	5.46
$\Delta G_{binding}$	-50.50	-44.22	-33.66

[b] $\Delta E_{pol,ele}$ is polar solvation plus electrostatic. All units are kcal/mol.

Table 3. Results of MM-GBSA method of R, H and G to TLR8[c].

Item	TLR8-H	TLR8-R	TLR8-G
van der Waals	-41.41	-38.32	-27.90
Electrostatic	74.98	27.72	157.83
Polar solvation	-70.10	-23.78	-146.77
Non-polar Solv.	-5.56	-5.16	-4.14
$\Delta E_{pol,ele}$	4.88	3.94	11.06
$\Delta G_{binding}$	-42.09	-39.54	-20.98

[c] $\Delta E_{pol,ele}$ is polar solvation plus electrostatic. All units are kcal/mol.

Fig 6(A-C) depicts the interaction plot of H, R and G with TLR7 pocket residues. There are electrostatic interactions, H-bond interactions, π-π interactions, and C-H-π interactions between Asp555, Thr586, Phe408 and Leu557 with agonists. Phe351, Tyr356, Val381 and Ile585 form the hydrophobic interaction regions. Compared with H and R, G forms a stronger H-bond interaction

bioRxiv preprint doi: https://doi.org/10.1101/2021.11.15.468604; this version posted November 15, 2021. The copyright holder for this preprint (which was not certified by peer review) is the author/funder, who has granted bioRxiv a license to display the preprint in perpetuity. It is made available under aCC-BY 4.0 International license.

with Thr586 of TLR7 through a nitrogen atom. However, the movement of the side chain weakens the van der Waals interactions between G and Phe351, Val381 and Ile585. The carbon atom on the side chain is more flexible and hydrophobic than the oxygen atom on the side chain, leading the molecule-H to be more adapted to pocket environment. It forms stronger electrostatic interactions with Asp555 and stronger van der Waals interaction with Val381 and Phe351.

Fig 6(D-F) depicts the interaction plot of H, R and G with of TLR8 pocket residues. There are electrostatic interactions, H-bond interactions and π-π interactions between Asp543, Thr574 and Phe405 with H and R. Tyr348, Tyr353, Val378 and Val573 form the hydrophobic interaction regions. Compared with H and R, G forms two electrostatic interactions with Asp545 and Asp543. However, this interaction weakens the H-bond interaction with Thr574 and Van der Waals interaction with Tyr348 and Val573. Zhu et al proposed that G is an agonist of TLR7 but not of human TLR8, which in accordance with our modeling. Using NF-κB reporter assay to measure the activation of human TLR7 and human TLR8, they found that G only activated human TLR7, but not human TLR8 in Cos-7 cells and 293T cells [89]. The carbon atom on the side chain is more flexible and hydrophobic than the oxygen atom on the side chain, leading the molecule-H to be more adapted to pocket environment. It forms stronger electrostatic interaction with Asp543 and stronger van der Waals interactions with Tyr353. The carbon atom on the side chain is more flexible and hydrophobic than the oxygen atom on the side chain, leading the molecule-H to be more adapted to pocket environment. It forms stronger electrostatic interaction with Asp543 and stronger van der Waals interactions with Tyr353.

The residue of TLR8 alignment to Leu557 of TLR7 is Asp545, which might result in a weaker interaction with agonists. Besides, Leu557 conserved in TLR7 has been reported to form an important C-H-π interaction with TLR7 [64].

bioRxiv preprint doi: https://doi.org/10.1101/2021.11.15.468604; this version posted November 15, 2021. The copyright holder for this preprint (which was not certified by peer review) is the author/funder, who has granted bioRxiv a license to display the preprint in perpetuity. It is made available under aCC-BY 4.0 International license.

Fig 6. The interactions between the agonists R, H and G against TLR7 and TLR8. TLR7-H system (A), TLR7-R system (B), TLR7-G system (C), TLR8-H system (D), TLR8-R system (E), TLR8-G system (F). The electrostatic interactions are shown in magentas dashes, the H-bond interactions are shown in yellow dashes, the π-π interactions are shown in green dashes, and the C-H-π interactions are shown in red dashes. TLR7 and TLR8 are shown in white cartoon. Agonists and representative residues are shown in orange and cyan stick.

3.4 Hydrogen bond interaction and van der Waals interaction between TLR7/8 and agonists

To further explore the interactions between three agonists and the receptors, the occupancy of hydrogen bonds with more than 10% occupancy between the agonists and residues atoms were analyzed to discard the extremely weak hydrogen bond interaction. The important atoms on the three agonists are shown in Fig 7C. The details of the hydrogen bond between agonists and TLR7 are shown in Fig 7A and Table S7-S12. In TLR7-H, TLR7-R and TLR7-G systems, the stable hydrogen bonds formed in Asp555 and N and N1 atoms on agonists were maintained during the last 20 ns of the conformations. In TLR7-H and TLR7-R systems, the occupancy of hydrogen bonds between Thr586 and N1 atoms on agonists (TLR7-H: 34.88%, TLR7-R: 43.83%) are similar. Nevertheless, the occupancy of the hydrogen bond between N1 and Thr586 of TLR7-G is very low (TLR7-G: 12.99%). Since N4 on G was protonated, a hydrogen bond formed between Thr586 of TLR7-G and N4, resulting in a change the orientation of the side chain and the loss of the hydrogen bond between Thr586 of TLR7-G and N2.

The details of the hydrogen bonds between three agonists and TLR8 are shown in Fig 7B and Table S12-S14. In TLR8-H, TLR8-R and TLR8-G systems, the stable hydrogen bonds formed in Asp543 and N and N1 atoms on agonists were maintained during the last 20 ns of the conformations. In TLR8-H and TLR8-R systems, the hydrogen bonds form between Thr574 of

bioRxiv preprint doi: https://doi.org/10.1101/2021.11.15.468604; this version posted November 15, 2021. The copyright holder for this preprint (which was not certified by peer review) is the author/funder, who has granted bioRxiv a license to display the preprint in perpetuity. It is made available under aCC-BY 4.0 International license.

TLR8 and N1 (TLR8-H: 30.68%, TLR8-R: 25.29%). The occupancy of hydrogen bond between N1 and Thr574 of TLR8-G is zero. Since N4 on G was protonated, hydrogen bond formed between G572 of TLR8-G and N4, which changed the orientation of the side chain.

Fig 7. Analysis of hydrogen bond interactions between three agonists and TLR7 and TLR8. Occupancy of hydrogen bonds between agonists and TLR7 (A) and TLR8 (B). (C) The position of the important atom on the agonists H, R and G.

The occupancy of residues less than 5 Å away from the agonists were analyzed in detail. To analyze the difference in data, all occupancy less than 20% or close to 100% in all six systems were ignored. The TLR7-R (Fig 8C) and TLR8-R (Fig 8D) systems are chosen to present the position relationship between residues and agonists. As shown in Fig 8A, the occupancy of residues Asn265, Phe349, Glu352, Leu353, Gln354, Gln379, Tyr380, Thr406, Asn407, Phe466, Tyr579 and His587 are highest in TLR7-H, lower in TLR7-R, and lowest in TLR7-G. Among them, residues Asn265, Phe349, Glu352, Leu353, Gln379, Tyr380, Thr406, Asn407 and Phe466 are located around the aliphatic tail. And as shown in Fig 8B, the occupancy of residues Phe261, Asn262, Phe346, Gly351, Gly376, Tyr377, Ile403 and Thr574 are highest in TLR8-H, lower in TLR8-R and lowest in TLR8-G. Among them, residues Phe261, Asn262, Phe346, Gly376, Tyr377 and Ile403 are located around the aliphatic tail. The above indicates that the occupancy of residues around three aliphatic tails are quite different, resulting in the van der Waals interaction between three agonists and receptors to be ranked H, R, then G, from highest to lowest. Comparing Fig 8A and Fig 8B, the residues Phe466 and Glu583 in TLR7 complex systems were located in the 5 Å range around the agonists for a certain period of time, while the occupancy of corresponding residues Pro463 and Ala571 in TLR8 complex system is zero. And the occupancy of residues Tyr264, Asn265, Leu353 and His587 in three TLR7 complex systems are higher than

bioRxiv preprint doi: https://doi.org/10.1101/2021.11.15.468604; this version posted November 15, 2021. The copyright holder for this preprint (which was not certified by peer review) is the author/funder, who has granted bioRxiv a license to display the preprint in perpetuity. It is made available under aCC-BY 4.0 International license.

369 residues Phe261, Asn262, Lys350, and His575 in three TLR8 complex systems, respectively. In
370 addition, the occupancy of residues Glu352, Leu556 and Thr586 in two or one TLR7 complex
371 systems is higher than Ile349, Phe544 and THr574 in TLR8 complex systems, and the occupancy
372 of residues in other TLR7 and TLR8 complex systems are similar. This explains why the van der
373 Waals interaction and binding affinity between agonists and TLR7 is stronger than TLR8. The
374 corresponding counterpart of the residue of TLR7 in Fig 8A is the residue of TLR8 in Fig 8B.

375

376

377 Fig 8. Occupancy of residues less than 5 Å away from the three agonists. TLR7 complex systems (A) and
378 TLR8 complex systems (B). Red labels of horizontal coordinate represent pockets residues around side
379 chain of agonists. The residues on x-axis of (A) are in alignment with that of (B). Position relationship
380 between these residues and agonist in TLR7-R system (C) and TLR8-R system (D). The residues are shown
381 in surface and stick. Red surface represents negative charge and blue surface represents positive charge.
382 Agonists are shown in cyan stick.

383

384 **Conclusion**

385 The aim of this research was to explore the intrinsic mechanisms underlying the selectivity
386 of R, H and G for TLR7 and TLR8 at atomic level. MD simulations and MM-GBSA method
387 were used to model the overall conformational changes and calculate the binding free energies
388 between three agonists and the TLR7 and TLR8. Trajectory analysis showed that TLR7-R and
389 TLR7-G systems form more “open” conformations during the simulation, however, other systems
390 kept in closed conformations. The pockets residues in TLR7 are conformationally less flexible
391 than those in TLR8, suggesting tight binding in TLR7. This is confirmed by the predicted binding
392 free energies via MMM-GBSA method. Plus, the calculated binding free energies indicated that
393 three agonists are more sensitive for TLR7 than TLR8, and the rank of the binding free energy

bioRxiv preprint doi: https://doi.org/10.1101/2021.11.15.468604; this version posted November 15, 2021. The copyright holder for this preprint (which was not certified by peer review) is the author/funder, who has granted bioRxiv a license to display the preprint in perpetuity. It is made available under aCC-BY 4.0 International license.

values are in agreement with the experimental EC50 values in the cellular assay. In brief, in the last 20 ns of the complex systems, the flexible and hydrophobic aliphatic side chain of H forms van der Waals interactions with Val381 and Phe351 of TLR7 and Tyr353 of TLR8. The side chain nitrogen of G is positively charged in an acidic environment, leading to its much less favorite interaction with Ile585 of TLR7 and Val573 of TLR8. Stable hydrogen bonds were formed between agonists and Asp555 of TLR7 and Asp 543 of TLR8. The occupancy of residues around less than 5 Å away from three agonists is quiet different, which account for the deviation of van der Waals interaction between agonists and receptors. An atomic difference on the aliphatic tail of each agonists results in the occupancy of residues and the change of van der Waals interaction. Thus, MD simulations provide explanation of differences in interaction modes of three agonists binding with TLR7 and TLR8 at the atomic level, paving the way for further design of more effective TLR7 and TLR8 modulators.

Note

The authors declare no competing financial interest.

Author Contributions

Conceptualization: Jinxia Nancy Deng, Steven Zhang

Data curation: Xiaoyu Wang

Formal Analysis: Xiaoyu Wang, Jinxia Nancy Deng, Yu Chen

Funding acquisition: Jinxia Nancy Deng

Investigation: Xiaoyu Wang, Yu Chen, Jinxia Nancy Deng

Methodology: Xiaoyu Wang, Jinxia Nancy Deng

Project administration: Jinxia Nancy Deng

Resources: Jinxia Nancy Deng

bioRxiv preprint doi: https://doi.org/10.1101/2021.11.15.468604; this version posted November 15, 2021. The copyright holder for this preprint (which was not certified by peer review) is the author/funder, who has granted bioRxiv a license to display the preprint in perpetuity. It is made available under aCC-BY 4.0 International license.

Supervision: Jinxia Nancy Deng

Validation: Xiaoyu Wang

Visualization: Xiaoyu Wang

Writing – original draft: Xiaoyu Wang, Yu Chen

Writing – review & editing: Jinxia Nancy Deng, Yu Chen, Steven Zhang, Xiaoyu Wang

References

1. Kawai T, Akira S (2011) Toll-like receptors and their crosstalk with other innate receptors in infection and immunity. Immunity 34: 637-650.

2. Gay NJ, Symmons MF, Gangloff M, Bryant CE (2014) Assembly and localization of Toll-like receptor signalling complexes. Nat Rev Immunol 14: 546-558.

3. Kawasaki T, Kawai T (2014) Toll-like receptor signaling pathways. Front Immunol 5: 461.

4. Sacre S, Lo A, Gregory B, Stephens M, Chamberlain G, et al. (2016) Oligodeoxynucleotide inhibition of Toll-like receptors 3, 7, 8, and 9 suppresses cytokine production in a human rheumatoid arthritis model. Eur J Immunol 46: 772-781.

5. Brentano F, Kyburz D, Gay S (2009) Toll-like receptors and rheumatoid arthritis. Methods Mol Biol 517: 329-343.

6. Roelofs MF, Joosten LA, Abdollahi-Roodsaz S, van Lieshout AW, Sprong T, et al. (2005) The expression of toll-like receptors 3 and 7 in rheumatoid arthritis synovium is increased and costimulation of toll-like receptors 3, 4, and 7/8 results in synergistic cytokine production by dendritic cells. Arthritis Rheum 52: 2313-2322.

7. Sheyhidin I, Nabi G, Hasim A, Zhang RP, Ainiwaer J, et al. (2011) Overexpression of TLR3, TLR4, TLR7 and TLR9 in esophageal squamous cell carcinoma. World J Gastroenterol 17: 3745-3751.

bioRxiv preprint doi: https://doi.org/10.1101/2021.11.15.468604; this version posted November 15, 2021. The copyright holder for this preprint (which was not certified by peer review) is the author/funder, who has granted bioRxiv a license to display the preprint in perpetuity. It is made available under aCC-BY 4.0 International license.

8. Komatsuda A, Wakui H, Iwamoto K, Ozawa M, Togashi M, et al. (2008) Up-regulated expression of Toll-like receptors mRNAs in peripheral blood mononuclear cells from patients with systemic lupus erythematosus. Clin Exp Immunol 152: 482-487.

9. Patel MC, Shirey KA, Pletneva LM, Boukhvalova MS, Garzino-Demo A, et al. (2014) Novel drugs targeting Toll-like receptors for antiviral therapy. Future Virol 9: 811-829.

10. Patinote C, Karroum NB, Moarbess G, Cirnat N, Kassab I, et al. (2020) Agonist and antagonist ligands of toll-like receptors 7 and 8: Ingenious tools for therapeutic purposes. Eur J Med Chem 193: 112238.

11. McGowan DC (2019) Latest advances in small molecule TLR 7/8 agonist drug research. Curr Top Med Chem 19: 2228-2238.

12. Agrawal S, Kandimalla ER (2007) Synthetic agonists of Toll-like receptors 7, 8 and 9. Biochem Soc Trans 35: 1461-1467.

13. Heil F, Hemmi H, Hochrein H, Ampenberger F, Kirschning C, et al. (2004) Species-specific recognition of single-stranded RNA via toll-like receptor 7 and 8. Science 303: 1526-1529.

14. Brown JN, Kohler JJ, Coberley CR, Sleasman JW, Goodenow MM (2008) HIV-1 activates macrophages independent of Toll-like receptors. PLoS One 3: e3664.

15. Beignon AS, McKenna K, Skoberne M, Manches O, DaSilva I, et al. (2005) Endocytosis of HIV-1 activates plasmacytoid dendritic cells via Toll-like receptor-viral RNA interactions. J Clin Invest 115: 3265-3275.

16. Cervantes-Barragan L, Zust R, Weber F, Spiegel M, Lang KS, et al. (2007) Control of coronavirus infection through plasmacytoid dendritic-cell-derived type I interferon. Blood 109: 1131-1137.

17. Hornung V, Rothenfusser S, Britsch S, Krug A, Jahrsdorfer B, et al. (2002) Quantitative expression of toll-like receptor 1-10 mRNA in cellular subsets of human peripheral blood

bioRxiv preprint doi: https://doi.org/10.1101/2021.11.15.468604; this version posted November 15, 2021. The copyright holder for this preprint (which was not certified by peer review) is the author/funder, who has granted bioRxiv a license to display the preprint in perpetuity. It is made available under aCC-BY 4.0 International license.

mononuclear cells and sensitivity to CpG oligodeoxynucleotides. J Immunol 168: 4531-4537.

18. Barr TA, Brown S, Ryan G, Zhao J, Gray D (2007) TLR-mediated stimulation of APC: Distinct cytokine responses of B cells and dendritic cells. Eur J Immunol 37: 3040-3053.

19. Edwards AD, Diebold SS, Slack EM, Tomizawa H, Hemmi H, et al. (2003) Toll-like receptor expression in murine DC subsets: lack of TLR7 expression by CD8 alpha+ DC correlates with unresponsiveness to imidazoquinolines. Eur J Immunol 33: 827-833.

20. Crozat K, Vivier E, Dalod M (2009) Crosstalk between components of the innate immune system: promoting anti-microbial defenses and avoiding immunopathologies. Immunol Rev 227: 129-149.

21. Mackman RL, Mish M, Chin G, Perry JK, Appleby T, et al. (2020) Discovery of GS-9688 (Selgantolimod) as a Potent and Selective Oral Toll-Like Receptor 8 Agonist for the Treatment of Chronic Hepatitis B. J Med Chem 63: 10188-10203.

22. Zhang Z, Ohto U, Shibata T, Krayukhina E, Taoka M, et al. (2016) Structural Analysis Reveals that Toll-like Receptor 7 Is a Dual Receptor for Guanosine and Single-Stranded RNA. Immunity 45: 737-748.

23. Tanji H, Ohto U, Shibata T, Taoka M, Yamauchi Y, et al. (2015) Toll-like receptor 8 senses degradation products of single-stranded RNA. Nat Struct Mol Biol 22: 109-115.

24. Diebold SS, Kaisho T, Hemmi H, Akira S, Reis e Sousa C (2004) Innate antiviral responses by means of TLR7-mediated recognition of single-stranded RNA. Science 303: 1529-1531.

25. Liu YJ (2005) IPC: professional type 1 interferon-producing cells and plasmacytoid dendritic cell precursors. Annu Rev Immunol 23: 275-306.

26. McCammon JA, Gelin BR, Karplus M (1977) Dynamics of folded proteins. Nature 267: 585-590.

bioRxiv preprint doi: https://doi.org/10.1101/2021.11.15.468604; this version posted November 15, 2021. The copyright holder for this preprint (which was not certified by peer review) is the author/funder, who has granted bioRxiv a license to display the preprint in perpetuity. It is made available under aCC-BY 4.0 International license.

27. Urbanc B, Betnel M, Cruz L, Bitan G, Teplow DB (2010) Elucidation of amyloid beta-protein oligomerization mechanisms: discrete molecular dynamics study. J Am Chem Soc 132: 4266-4280.

28. Gsponer J, Haberthür U, Caflisch A (2003) The role of side-chain interactions in the early steps of aggregation: Molecular dynamics simulations of an amyloid-forming peptide from the yeast prion Sup35. Proc Natl Acad Sci U S A 100: 5154-5159.

29. Lemkul JA, Bevan DR (2010) Assessing the stability of Alzheimer's amyloid protofibrils using molecular dynamics. J Phys Chem B 114: 1652-1660.

30. Woods CJ, Malaisree M, Pattarapongdilok N, Sompornpisut P, Hannongbua S, et al. (2012) Long time scale GPU dynamics reveal the mechanism of drug resistance of the dual mutant I223R/H275Y neuraminidase from H1N1-2009 influenza virus. Biochemistry 51: 4364-4375.

31. Phanich J, Rungrotmongkol T, Kungwan N, Hannongbua S (2016) Role of R292K mutation in influenza H7N9 neuraminidase toward oseltamivir susceptibility: MD and MM/PB(GB)SA study. J Comput Aided Mol Des 30: 917-926.

32. Yu Y, Wang J, Shao Q, Shi J, Zhu W (2015) Effects of drug-resistant mutations on the dynamic properties of HIV-1 protease and inhibition by Amprenavir and Darunavir. Sci Rep 5: 10517.

33. Campos SR, Machuqueiro M, Baptista AM (2010) Constant-pH molecular dynamics simulations reveal a β-rich form of the human prion protein. J Phys Chem B 114: 12692-12700.

34. Chen W, van der Kamp MW, Daggett V (2014) Structural and dynamic properties of the human prion protein. Biophys J 106: 1152-1163.

35. Sousa SF, Tamames B, Fernandes PA, Ramos MJ (2011) Detailed atomistic analysis of the HIV-1 protease interface. J Phys Chem B 115: 7045-7057.

bioRxiv preprint doi: https://doi.org/10.1101/2021.11.15.468604; this version posted November 15, 2021. The copyright holder for this preprint (which was not certified by peer review) is the author/funder, who has granted bioRxiv a license to display the preprint in perpetuity. It is made available under aCC-BY 4.0 International license.

520 36. Viricel C, Ahmed M, Barakat K (2015) Human PD-1 binds differently to its human ligands: a
521 comprehensive modeling study. J Mol Graph Model 57: 131-142.
522 37. Etheve L, Martin J, Lavery R (2016) Protein-DNA interfaces: a molecular dynamics analysis
523 of time-dependent recognition processes for three transcription factors. Nucleic Acids
524 Res 44: 9990-10002.
525 38. Schames JR, Henchman RH, Siegel JS, Sotriffer CA, Ni H, et al. (2004) Discovery of a novel
526 binding trench in HIV integrase. J Med Chem 47: 1879-1881.
527 39. Durrant JD, Keränen H, Wilson BA, McCammon JA (2010) Computational identification of
528 uncharacterized cruzain binding sites. PLoS Negl Trop Dis 4: e676.
529 40. Grant BJ, Lukman S, Hocker HJ, Sayyah J, Brown JH, et al. (2011) Novel allosteric sites on
530 Ras for lead generation. PLoS One 6: e25711.
531 41. Ivetac A, McCammon JA (2010) Mapping the druggable allosteric space of G-protein
532 coupled receptors: a fragment-based molecular dynamics approach. Chem Biol Drug Des
533 76: 201-217.
534 42. Lin JH, Perryman AL, Schames JR, McCammon JA (2002) Computational drug design
535 accommodating receptor flexibility: the relaxed complex scheme. J Am Chem Soc 124:
536 5632-5633.
537 43. Amaro RE, Schnaufer A, Interthal H, Hol W, Stuart KD, et al. (2008) Discovery of drug-like
538 inhibitors of an essential RNA-editing ligase in Trypanosoma brucei. Proc Natl Acad Sci
539 U S A 105: 17278-17283.
540 44. Durrant JD, Hall L, Swift RV, Landon M, Schnaufer A, et al. (2010) Novel naphthalene-
541 based inhibitors of Trypanosoma brucei RNA editing ligase 1. PLoS Negl Trop Dis 4:
542 e803.
543 45. Durrant JD, Urbaniak MD, Ferguson MA, McCammon JA (2010) Computer-aided
544 identification of Trypanosoma brucei uridine diphosphate galactose 4'-epimerase

bioRxiv preprint doi: https://doi.org/10.1101/2021.11.15.468604; this version posted November 15, 2021. The copyright holder for this preprint (which was not certified by peer review) is the author/funder, who has granted bioRxiv a license to display the preprint in perpetuity. It is made available under aCC-BY 4.0 International license.

545 inhibitors: toward the development of novel therapies for African sleeping sickness. J
546 Med Chem 53: 5025-5032.
547 46. Durrant JD, Cao R, Gorfe AA, Zhu W, Li J, et al. (2011) Non-bisphosphonate inhibitors of
548 isoprenoid biosynthesis identified via computer-aided drug design. Chem Biol Drug Des
549 78: 323-332.
550 47. Wang Y, Hess TN, Jones V, Zhou JZ, McNeil MR, et al. (2011) Novel inhibitors of
551 Mycobacterium tuberculosis dTDP-6-deoxy-L-lyxo-4-hexulose reductase (RmlD)
552 identified by virtual screening. Bioorg Med Chem Lett 21: 7064-7067.
553 48. Hucke O, Coulombe R, Bonneau P, Bertrand-Laperle M, Brochu C, et al. (2014) Molecular
554 dynamics simulations and structure-based rational design lead to allosteric HCV NS5B
555 polymerase thumb pocket 2 inhibitor with picomolar cellular replicon potency. J Med
556 Chem 57: 1932-1943.
557 49. Rastelli G, Ferrari AM, Costantino L, Gamberini MC (2002) Discovery of new inhibitors of
558 aldose reductase from molecular docking and database screening. Bioorg Med Chem 10:
559 1437-1450.
560 50. Distinto S, Yáñez M, Alcaro S, Cardia MC, Gaspari M, et al. (2012) Synthesis and biological
561 assessment of novel 2-thiazolylhydrazones and computational analysis of their
562 recognition by monoamine oxidase B. Eur J Med Chem 48: 284-295.
563 51. Zhao G, Perilla JR, Yufenyuy EL, Meng X, Chen B, et al. (2013) Mature HIV-1 capsid
564 structure by cryo-electron microscopy and all-atom molecular dynamics. Nature 497:
565 643-646.
566 52. Freddolino PL, Arkhipov AS, Larson SB, McPherson A, Schulten K (2006) Molecular
567 dynamics simulations of the complete satellite tobacco mosaic virus. Structure 14: 437-
568 439.
569 53. Zink M, Grubmüller H (2009) Mechanical properties of the icosahedral shell of southern bean
570 mosaic virus: a molecular dynamics study. Biophys J 96: 1350-1363.

bioRxiv preprint doi: https://doi.org/10.1101/2021.11.15.468604; this version posted November 15, 2021. The copyright holder for this preprint (which was not certified by peer review) is the author/funder, who has granted bioRxiv a license to display the preprint in perpetuity. It is made available under aCC-BY 4.0 International license.

571 54. Sanbonmatsu KY, Tung CS (2007) High performance computing in biology: multimillion
572 atom simulations of nanoscale systems. J Struct Biol 157: 470-480.
573 55. Freddolino PL, Liu F, Gruebele M, Schulten K (2008) Ten-microsecond molecular dynamics
574 simulation of a fast-folding WW domain. Biophys J 94: L57-L77.
575 56. Freddolino PL, Schulten K (2009) Common structural transitions in explicit-solvent
576 simulations of villin headpiece folding. Biophys J 97: 2338-2347.
577 57. Klepeis JL, Lindorff-Larsen K, Dror RO, Shaw DE (2009) Long-timescale molecular
578 dynamics simulations of protein structure and function. Curr Opin Struct Biol 19: 120-
579 127.
580 58. Kaur R, Arora N, Jamakhani MA, Malik S, Kumar P, et al. (2020) Development of multi-
581 epitope chimeric vaccine against Taenia solium by exploring its proteome: an in silico
582 approach. Expert Rev Vaccines 19: 105-114.
583 59. Ojha R, Pandey RK, Prajapati VK (2020) Vaccinomics strategy to concoct a promising
584 subunit vaccine for visceral leishmaniasis targeting sandfly and leishmania antigens. Int J
585 Biol Macromol 156: 548-557.
586 60. Patra MC, Batool M, Haseeb M, Choi S (2020) A Computational Probe into the Structure and
587 Dynamics of the Full-Length Toll-Like Receptor 3 in a Phospholipid Bilayer. Int J Mol
588 Sci 21: 2857.
589 61. Kubarenko A, Frank M, Weber AN (2007) Structure-function relationships of Toll-like
590 receptor domains through homology modelling and molecular dynamics. Biochem Soc
591 Trans 35: 1515-1518.
592 62. Mahita J, Sowdhamini R (2018) Investigating the effect of key mutations on the
593 conformational dynamics of toll-like receptor dimers through molecular dynamics
594 simulations and protein structure networks. Proteins 86: 475-490.

bioRxiv preprint doi: https://doi.org/10.1101/2021.11.15.468604; this version posted November 15, 2021. The copyright holder for this preprint (which was not certified by peer review) is the author/funder, who has granted bioRxiv a license to display the preprint in perpetuity. It is made available under aCC-BY 4.0 International license.

595 63. Tseng CY, Gajewski M, Danani A, Tuszynski JA (2014) Homology and molecular dynamics
596 models of toll-like receptor 7 protein and its dimerization. Chem Biol Drug Des 83: 656-
597 665.
598 64. Gentile F, Deriu MA, Licandro G, Prunotto A, Danani A, et al. (2015) Structure Based
599 Modeling of Small Molecules Binding to the TLR7 by Atomistic Level Simulations.
600 Molecules 20: 8316-8340.
601 65. Huang S, Mei H, Chen L, Shi T, Kuang Z, et al. (2020) Computational insight into the
602 conformational transition of human toll-like receptor 8 in the agonist-induced activation
603 processes. J Biomol Struct Dyn 38: 5537-5543.
604 66. Hemmi H, Kaisho T, Takeuchi O, Sato S, Sanjo H, et al. (2002) Small anti-viral compounds
605 activate immune cells via the TLR7 MyD88-dependent signaling pathway. Nat Immunol
606 3: 196-200.
607 67. Jurk M, Heil F, Vollmer J, Schetter C, Krieg AM, et al. (2002) Human TLR7 or TLR8
608 independently confer responsiveness to the antiviral compound R-848. Nat Immunol 3:
609 499.
610 68. Ganapathi L, Van Haren S, Dowling DJ, Bergelson I, Shukla NM, et al. (2015) The
611 Imidazoquinoline Toll-Like Receptor-7/8 Agonist Hybrid-2 Potently Induces Cytokine
612 Production by Human Newborn and Adult Leukocytes. PLoS One 10: e0134640.
613 69. Ma F, Zhang J, Zhang J, Zhang C (2010) The TLR7 agonists imiquimod and gardiquimod
614 improve DC-based immunotherapy for melanoma in mice. Cell Mol Immunol 7: 381-388.
615 70. Tanji H, Ohto U, Shibata T, Miyake K, Shimizu T (2013) Structural reorganization of the
616 Toll-like receptor 8 dimer induced by agonistic ligands. Science 339: 1426-1429.
617 71. Waterhouse A, Bertoni M, Bienert S, Studer G, Tauriello G, et al. (2018) SWISS-MODEL:
618 homology modelling of protein structures and complexes. Nucleic Acids Res 46: W296-
619 W303.

bioRxiv preprint doi: https://doi.org/10.1101/2021.11.15.468604; this version posted November 15, 2021. The copyright holder for this preprint (which was not certified by peer review) is the author/funder, who has granted bioRxiv a license to display the preprint in perpetuity. It is made available under aCC-BY 4.0 International license.

620 72. Hipp MM, Shepherd D, Gileadi U, Aichinger MC, Kessler BM, et al. (2013) Processing of
621 human toll-like receptor 7 by furin-like proprotein convertases is required for its
622 accumulation and activity in endosomes. Immunity 39: 711-721.
623 73. Tojo S, Zhang Z, Matsui H, Tahara M, Ikeguchi M, et al. (2020) Structural analysis reveals
624 TLR7 dynamics underlying antagonism. Nat Commun 11: 5204.
625 74. Gibbard RJ, Morley PJ, Gay NJ (2006) Conserved features in the extracellular domain of
626 human toll-like receptor 8 are essential for pH-dependent signaling. J Biol Chem 281:
627 27503-27511.
628 75. Schrödinger Release 2019-4: Maestro, Schrödinger, LLC: New York, NY, 2019.
629 76. Hess B, Kutzner C, van der Spoel D, Lindahl E (2008) GROMACS 4: Algorithms for highly
630 efficient, load-balanced, and scalable molecular simulation. J Chem Theory Comput 4:
631 435-447.
632 77. Hornak V, Abel R, Okur A, Strockbine B, Roitberg A, et al. (2006) Comparison of multiple
633 Amber force fields and development of improved protein backbone parameters. Proteins
634 65: 712-725.
635 78. Wang J, Wolf RM, Caldwell JW, Kollman PA, Case DA (2004) Development and testing of a
636 general amber force field. J Comput Chem 25: 1157-1174.
637 79. Jorgensen WL, Chandrasekhar J, Madura JD, Impey RW, Klein ML (1983) Comparison of
638 simple potential functions for simulating liquid water. J Chem Phys 79: 926-935.
639 80. Bussi G, Donadio D, Parrinello M (2007) Canonical sampling through velocity rescaling. J
640 Chem Phys 126: 014101.
641 81. Parrinello M, Rahman A (1981) Polymorphic transitions in single crystals: a new molecular
642 dynamics method. J Appl Phys 52: 7182-7190.
643 82. Hess B, Bekker H, Berendsen HJ, Fraaije JG (1997) LINCS: a linear constraint solver for
644 molecular simulations. J Comput Chem 18: 1463-1472.

bioRxiv preprint doi: https://doi.org/10.1101/2021.11.15.468604; this version posted November 15, 2021. The copyright holder for this preprint (which was not certified by peer review) is the author/funder, who has granted bioRxiv a license to display the preprint in perpetuity. It is made available under aCC-BY 4.0 International license.

645 83. Onufriev A, Bashford D, Case DA (2000) Modification of the generalized Born model
646 suitable for macromolecules. J Phys Chem B 104: 3712-3720.
647 84. Berhanu WM, Hansmann UH (2013) The stability of cylindrin beta-barrel amyloid oligomer
648 models-a molecular dynamics study. Proteins 81: 1542-1555.
649 85. Zhang T, Zhang J, Derreumaux P, Mu Y (2013) Molecular mechanism of the inhibition of
650 EGCG on the Alzheimer Abeta(1-42) dimer. J Phys Chem B 117: 3993-4002.
651 86. Humphrey W, Dalke A, Schulten K (1996) VMD: visual molecular dynamics. J Mol Graph
652 14: 33-38.
653 87. Shi C, Xiong Z, Chittepu P, Aldrich CC, Ohlfest JR, et al. (2012) Discovery of
654 Imidazoquinolines with Toll-Like Receptor 7/8 Independent Cytokine Induction. ACS
655 Med Chem Lett 3: 501-504.
656 88. Shukla NM, Malladi SS, Mutz CA, Balakrishna R, David SA (2010) Structure-activity
657 relationships in human toll-like receptor 7-active imidazoquinoline analogues. J Med
658 Chem 53: 4450-4465.
659 89. Zhu J, Lai K, Brownile R, Babiuk LA, Mutwiri GK (2008) Porcine TLR8 and TLR7 are both
660 activated by a selective TLR7 ligand, imiquimod. Mol Immunol 45: 3238-3243.

661

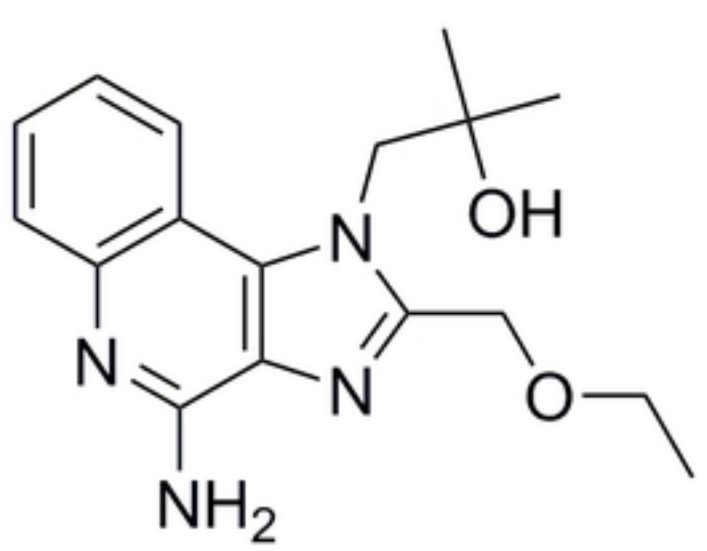

Resiquimod (R)

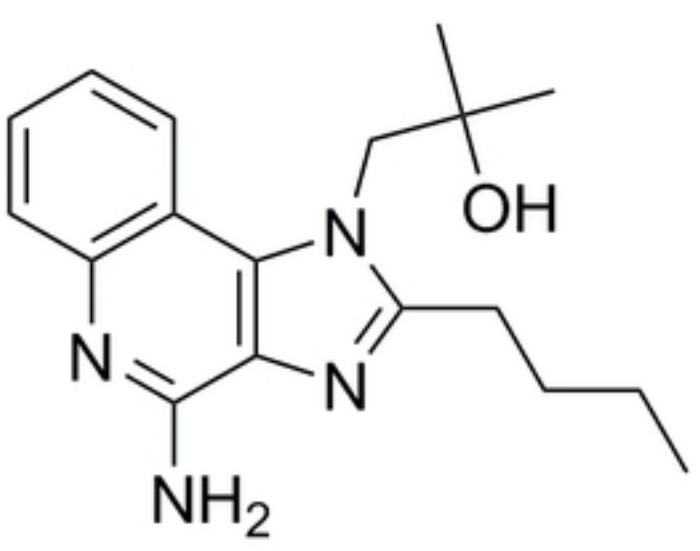

Hybrid-2 (H)

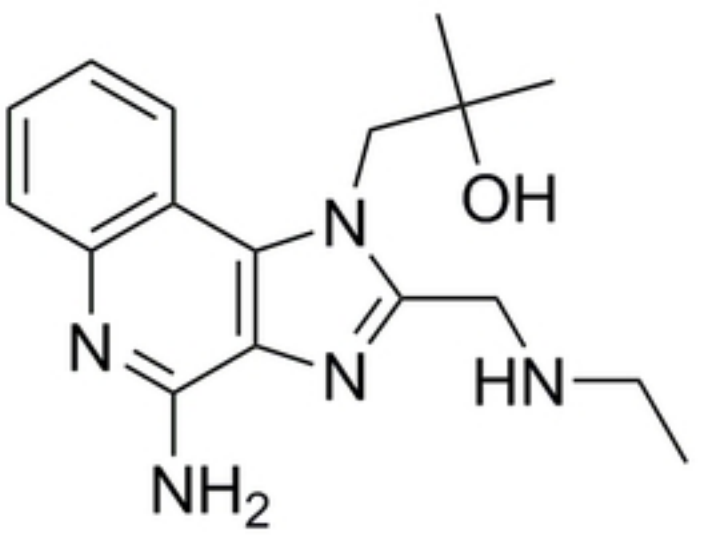

Gardiquimod (G)

Fig1

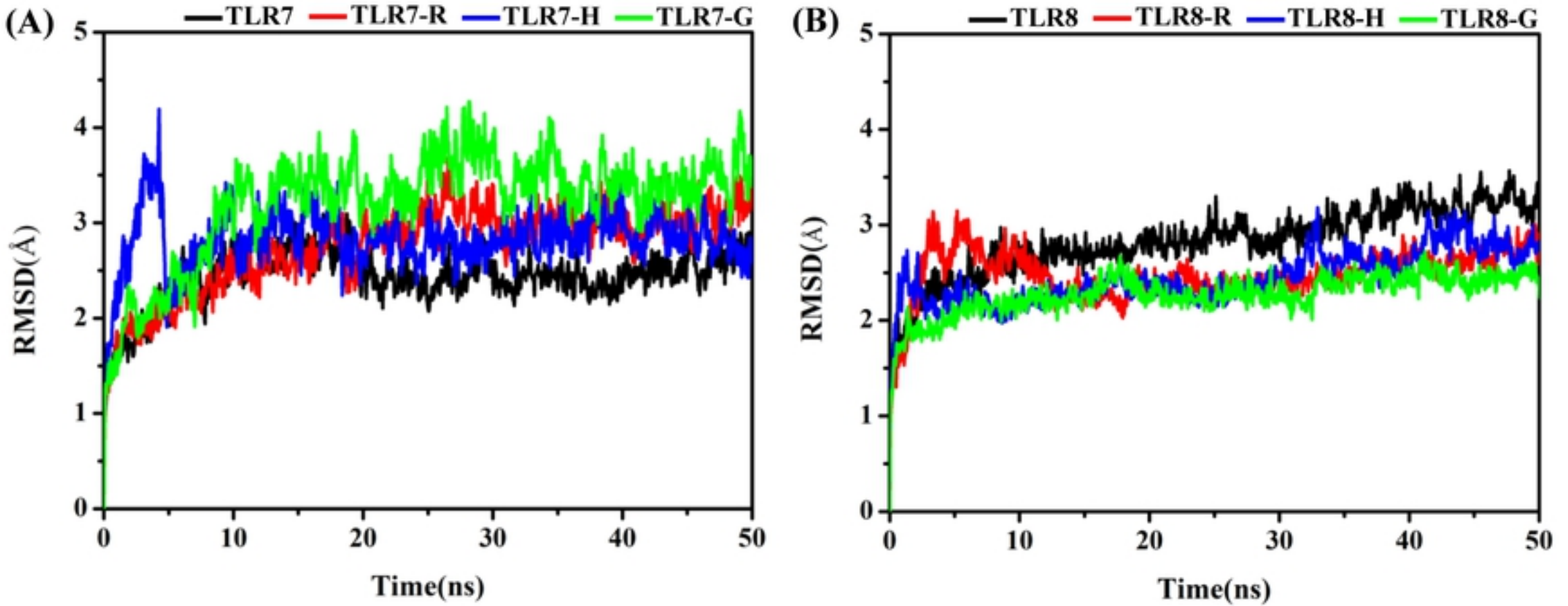
(A)
TLR7
TLR7-R
TLR7-H
TLR7-G
RMSD(Å)
Time(ns)
(B)
TLR8
TLR8-R
TLR8-H
TLR8-G
RMSD(Å)
Time(ns)

Fig2

bioRxiv preprint doi: https://doi.org/10.1101/2021.11.15.468604; this version posted November 15, 2021. The copyright holder for this preprint (which was not certified by peer review) is the author/funder, who has granted bioRxiv a license to display the preprint in perpetuity. It is made available under aCC-BY 4.0 International license.

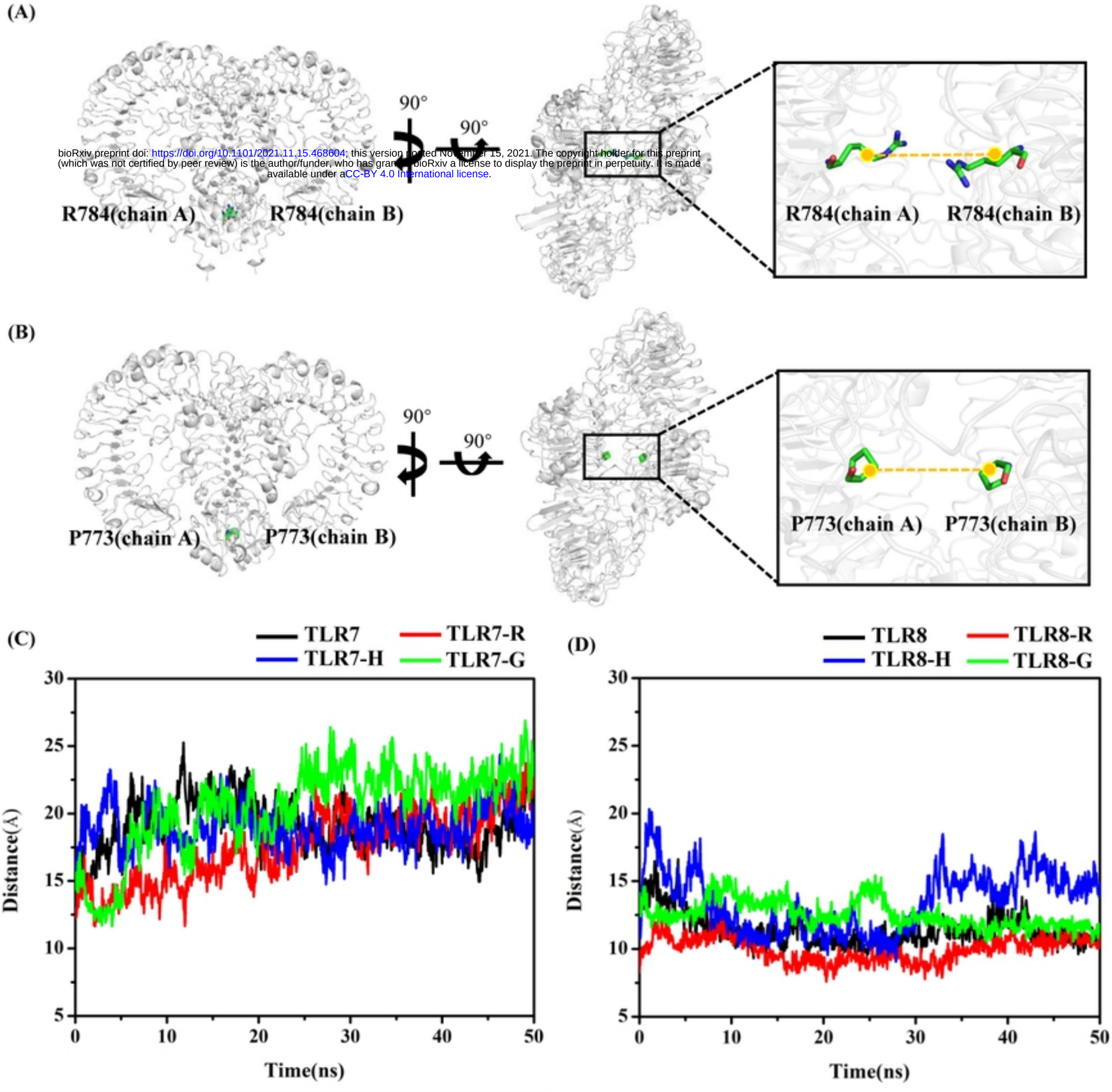

Fig3

bioRxiv preprint doi: https://doi.org/10.1101/2021.11.15.468604; this version posted November 15, 2021. The copyright holder for this preprint (which was not certified by peer review) is the author/funder, who has granted bioRxiv a license to display the preprint in perpetuity. It is made available under aCC-BY 4.0 International license.

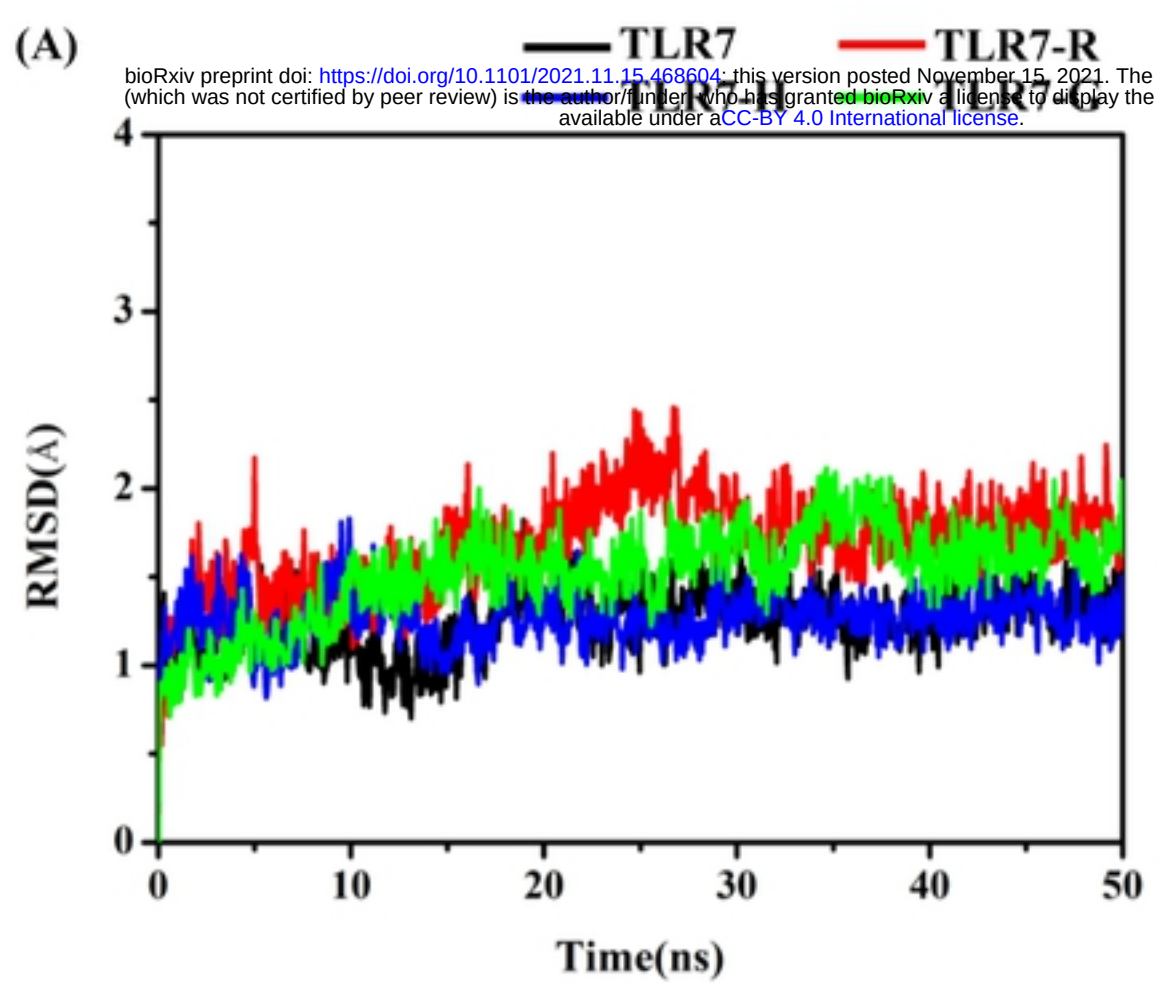

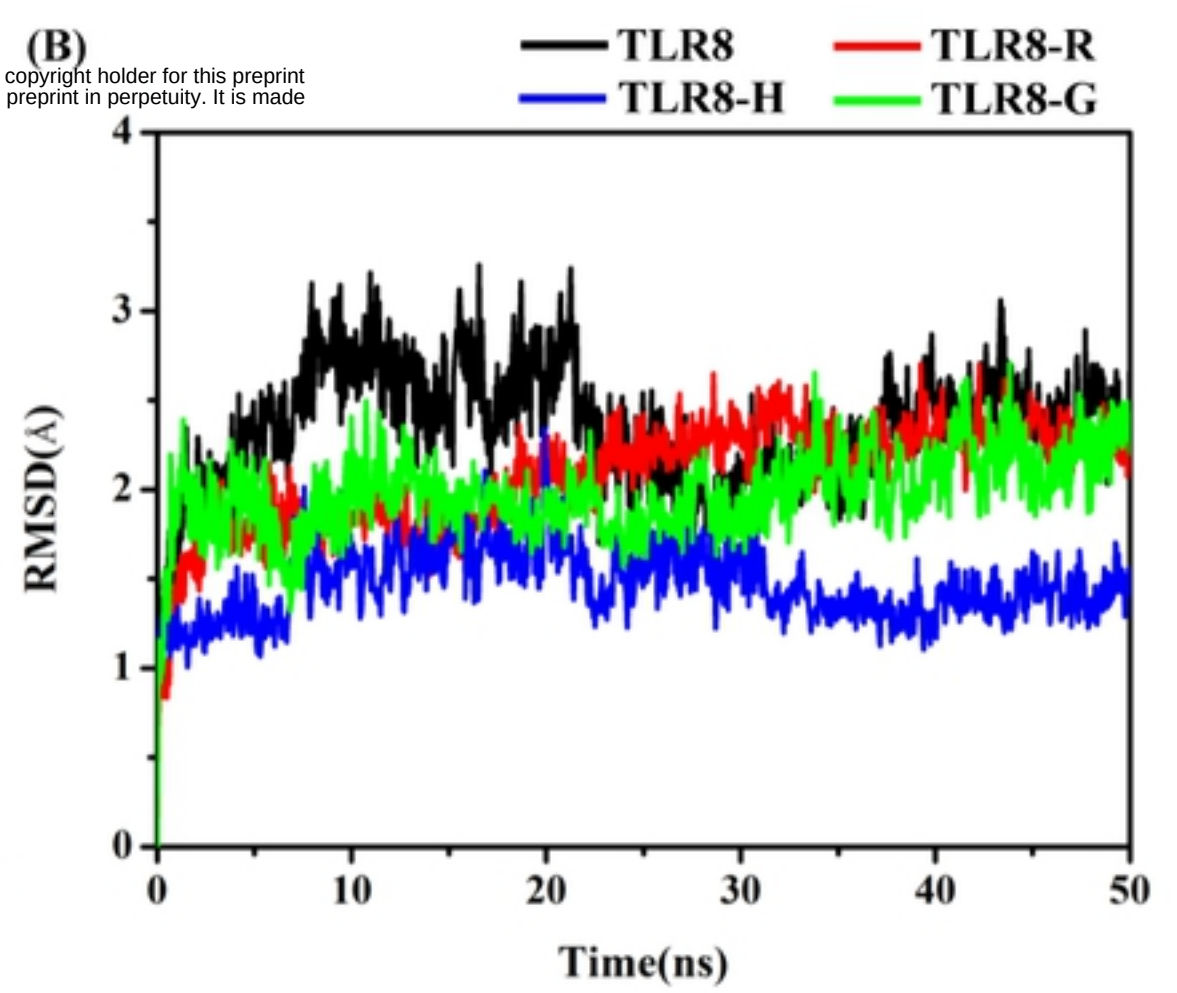

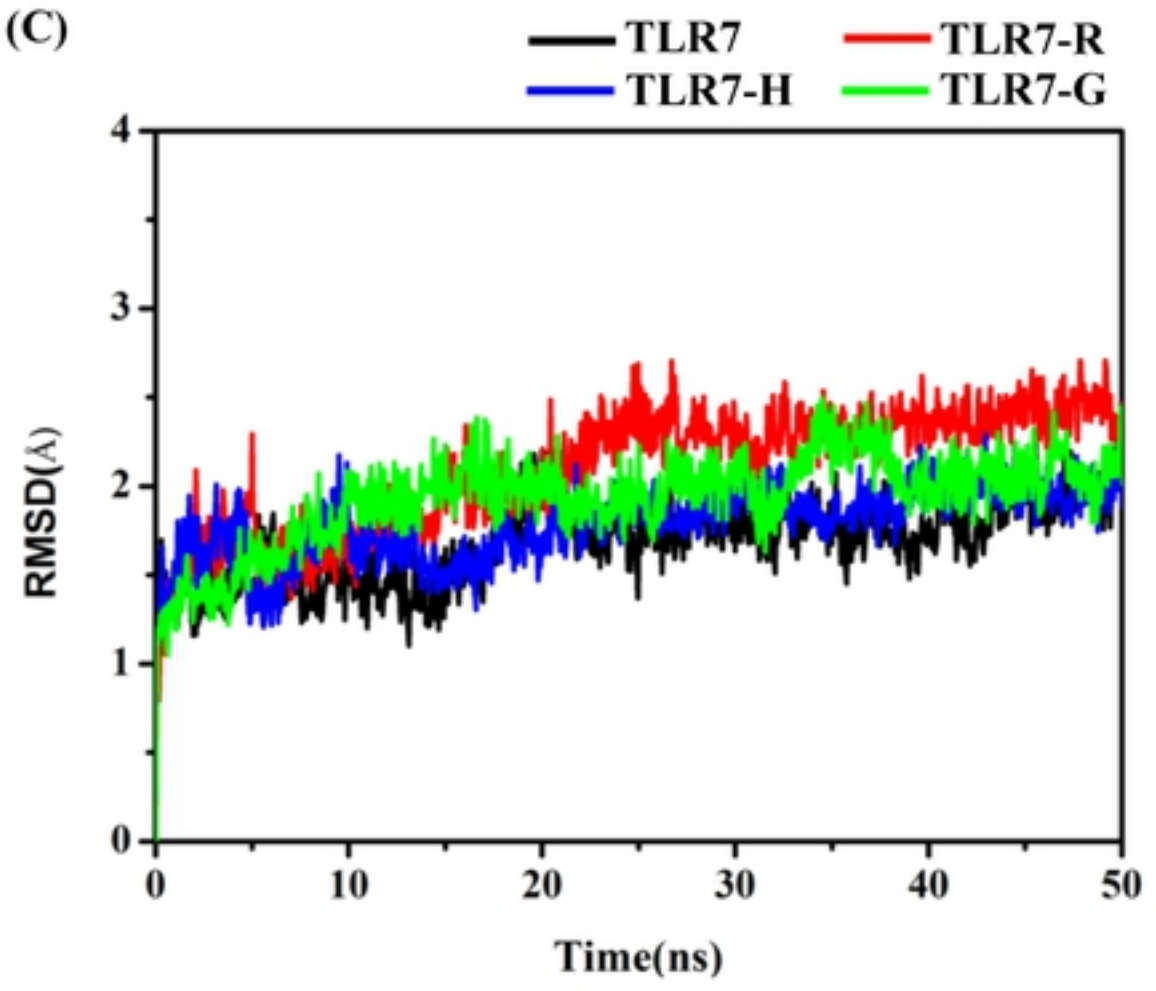

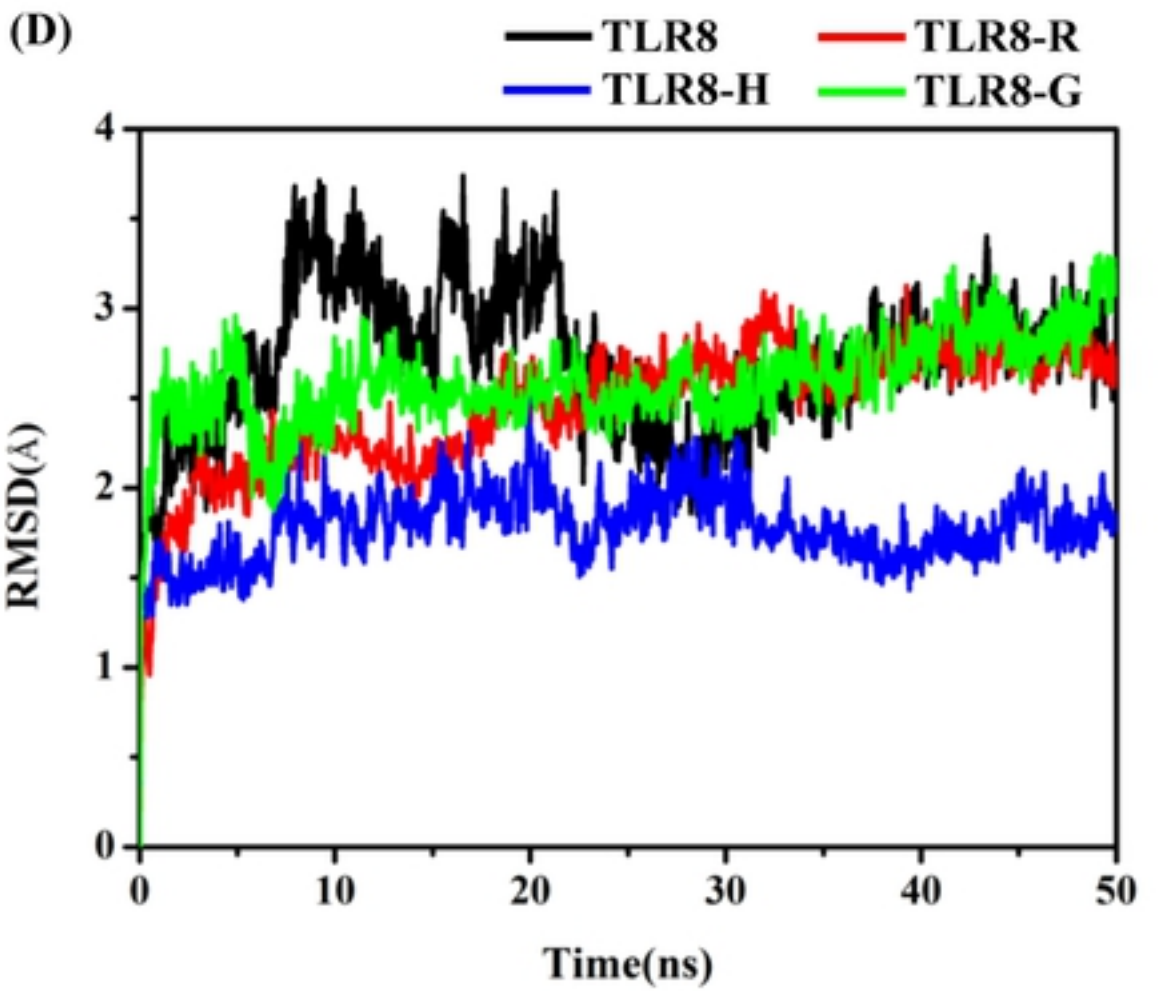

Fig4

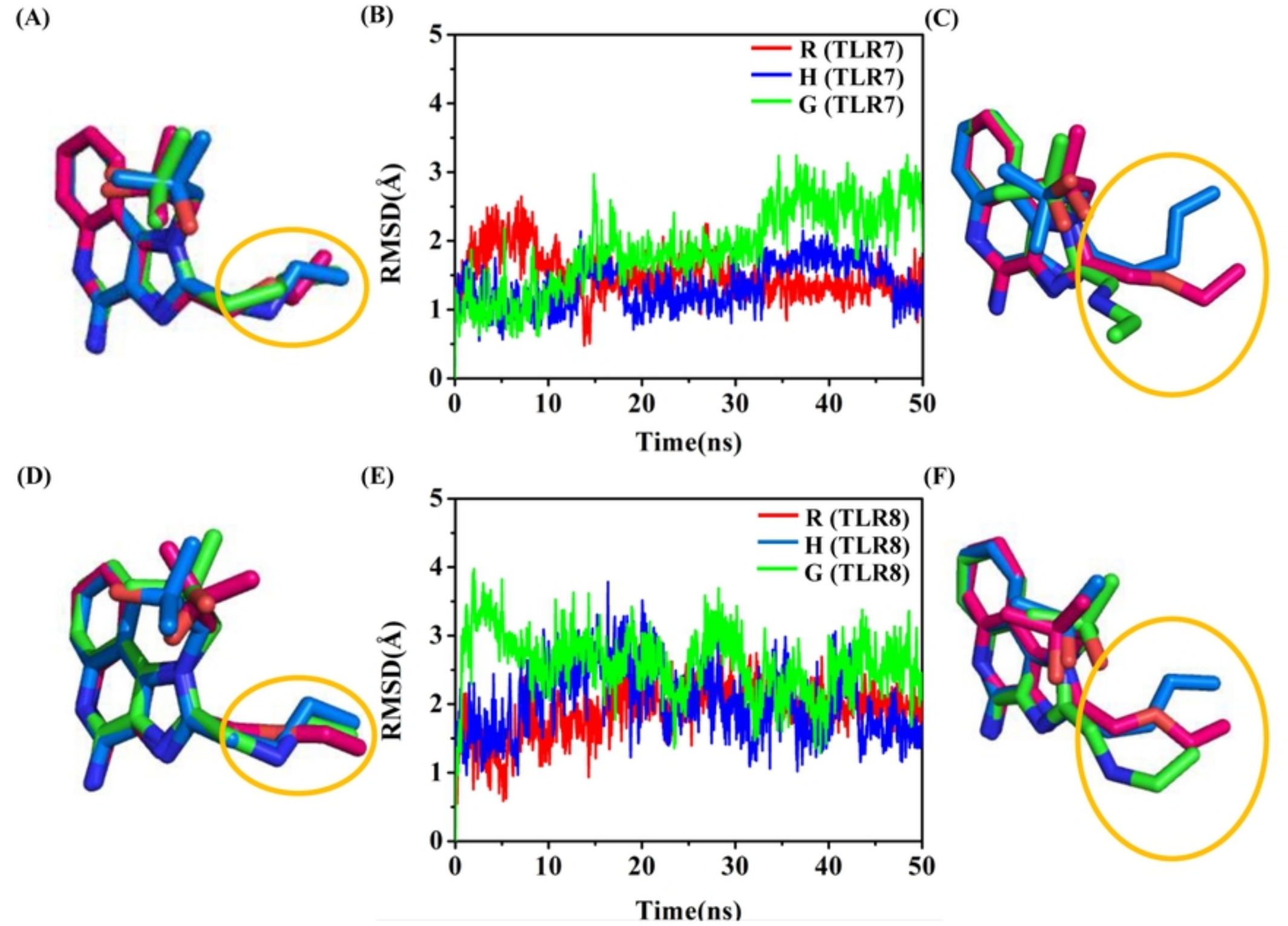
(A)
(B)
(C)
R (TLR7)
H (TLR7)
G (TLR7)
RMSD(Å)
Time(ns)
0
10
20
30
40
50
1
2
3
4
5
(D)
(E)
(F)
R (TLR8)
H (TLR8)
G (TLR8)
RMSD(Å)
Time(ns)

Fig5

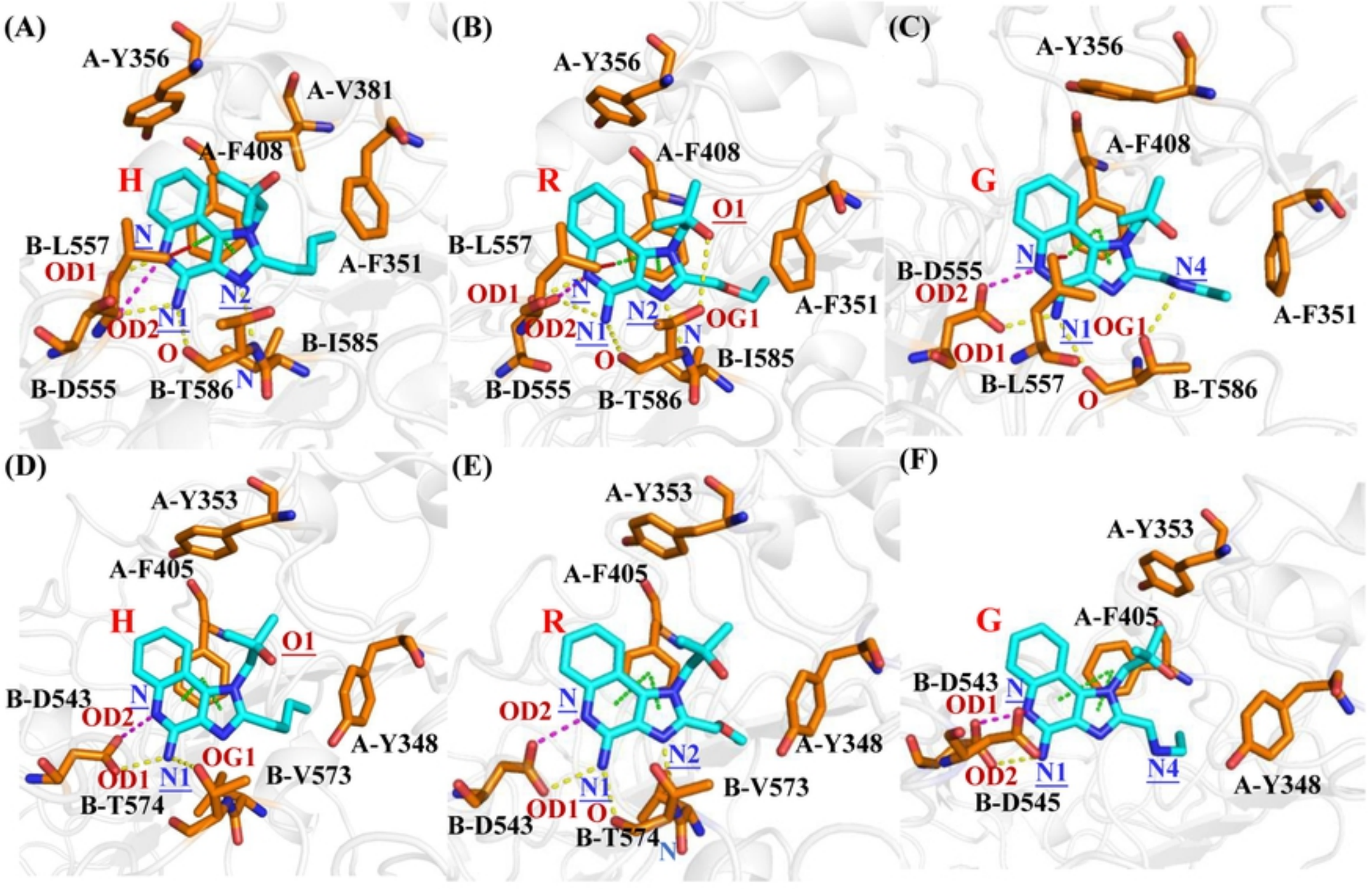
(A)
A-Y356
A-V381
A-F408
H
B-L557
N
OD1
A-F351
N2
OD2
N1
B-I585
O
B-D555
B-T586
N
(B)
A-Y356
A-F408
R
O1
B-L557
OD1
N
N2
A-F351
OD2
N1
OG1
N
B-I585
O
B-D555
B-T586
(C)
A-Y356
A-F408
G
N
N4
B-D555
OD2
A-F351
N1
OG1
OD1
B-L557
B-T586
O
(D)
A-Y353
A-F405
H
O1
B-D543
N
OD2
A-Y348
OG1
OD1
N1
B-V573
B-T574
(E)
A-Y353
A-F405
R
OD2
N
A-Y348
N2
N1
B-V573
OD1
O
B-D543
B-T574
N
(F)
A-Y353
G
A-F405
B-D543
N
OD1
N4
OD2
N1
A-Y348
B-D545

Fig6

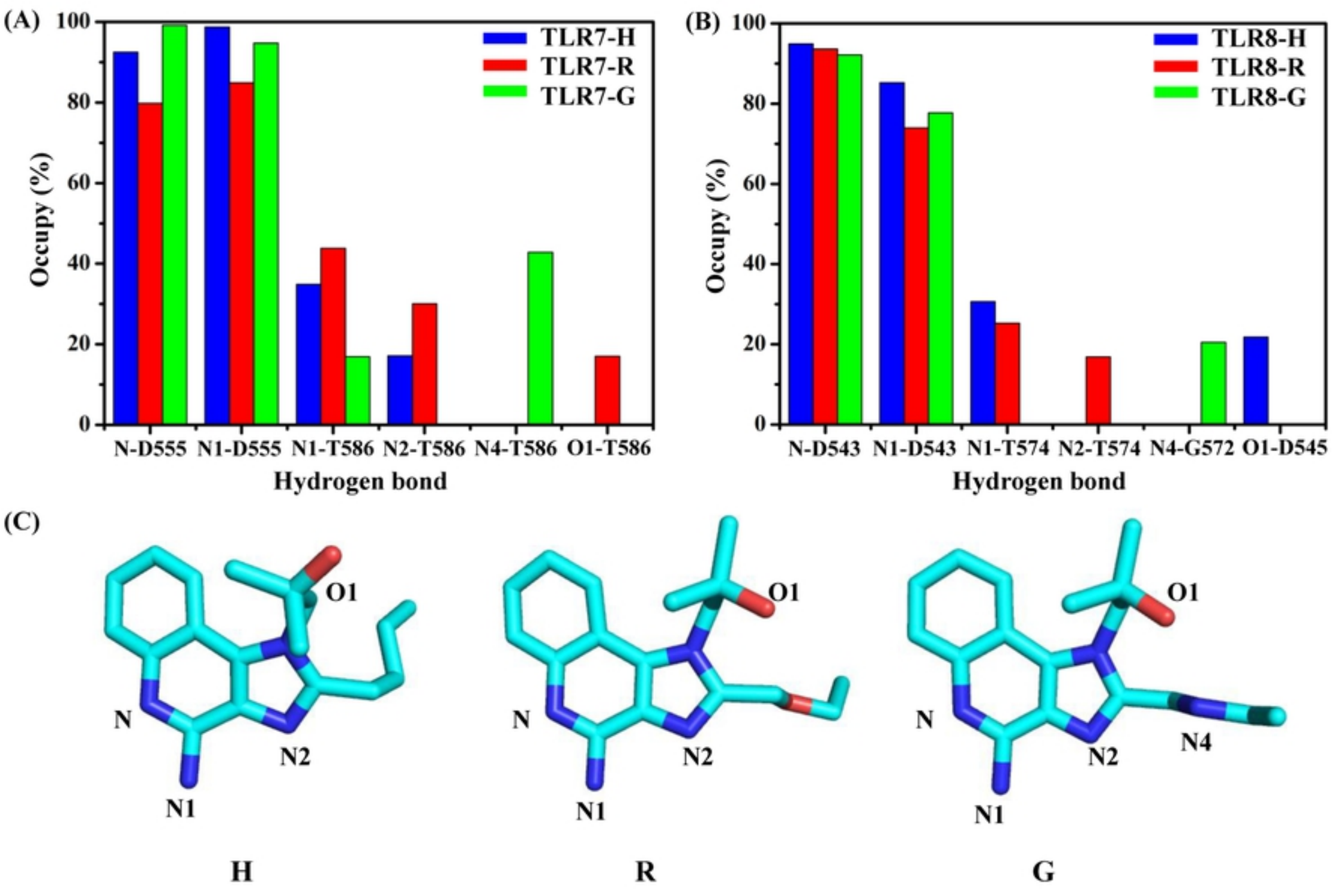
(A)
Occupy (%)
TLR7-H
TLR7-R
TLR7-G
N-D555
N1-D555
N1-T586
N2-T586
N4-T586
O1-T586
Hydrogen bond
(B)
TLR8-H
TLR8-R
TLR8-G
N-D543
N1-D543
N1-T574
N2-T574
N4-G572
O1-D545
Hydrogen bond
(C)
O1
N
N2
N1
H
R
N4
G

Fig7

bioRxiv preprint doi: https://doi.org/10.1101/2021.11.15.468686; this version posted November 15, 2021. The copyright holder for this preprint (which was not certified by peer review) is the author/funder, who has granted bioRxiv a license to display the preprint in perpetuity. It is made available under aCC-BY 4.0 International license.

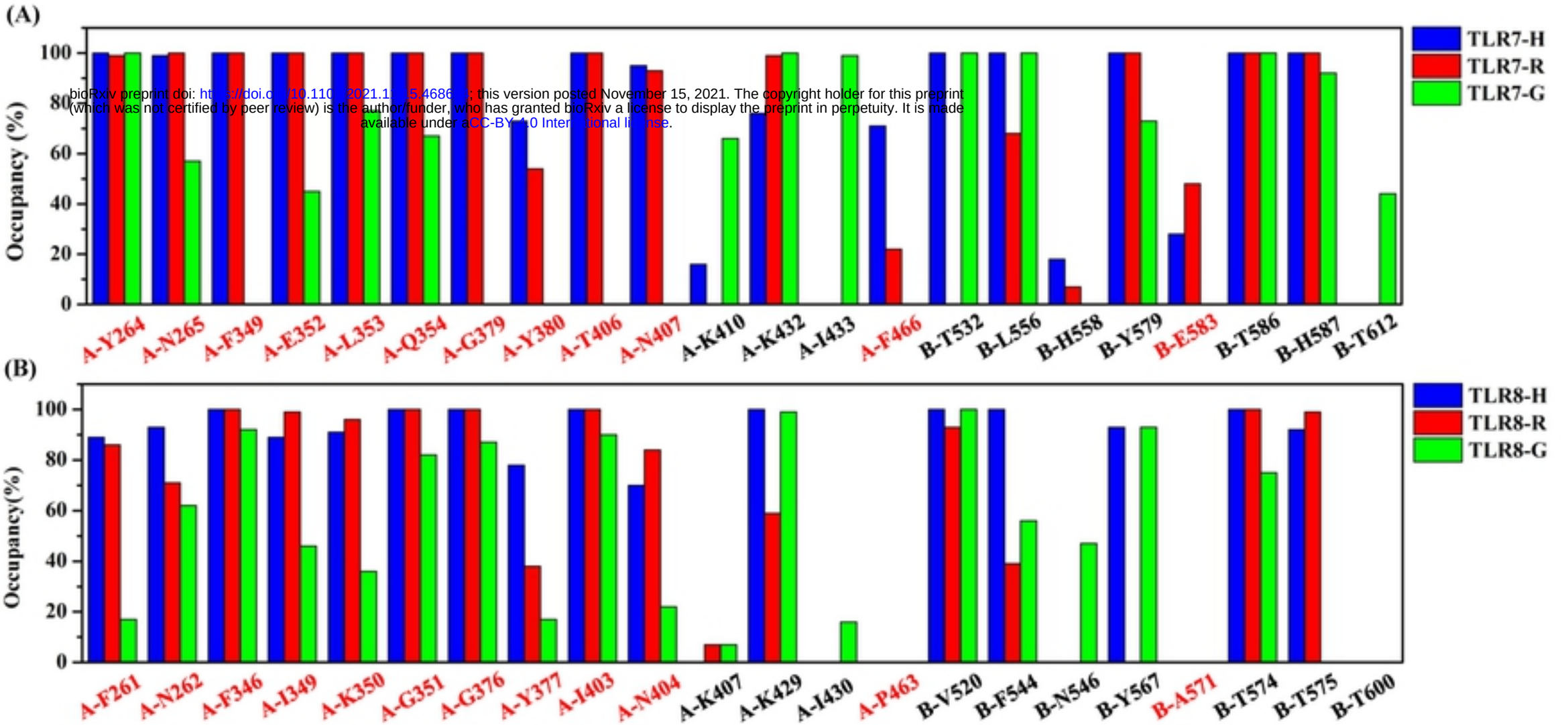

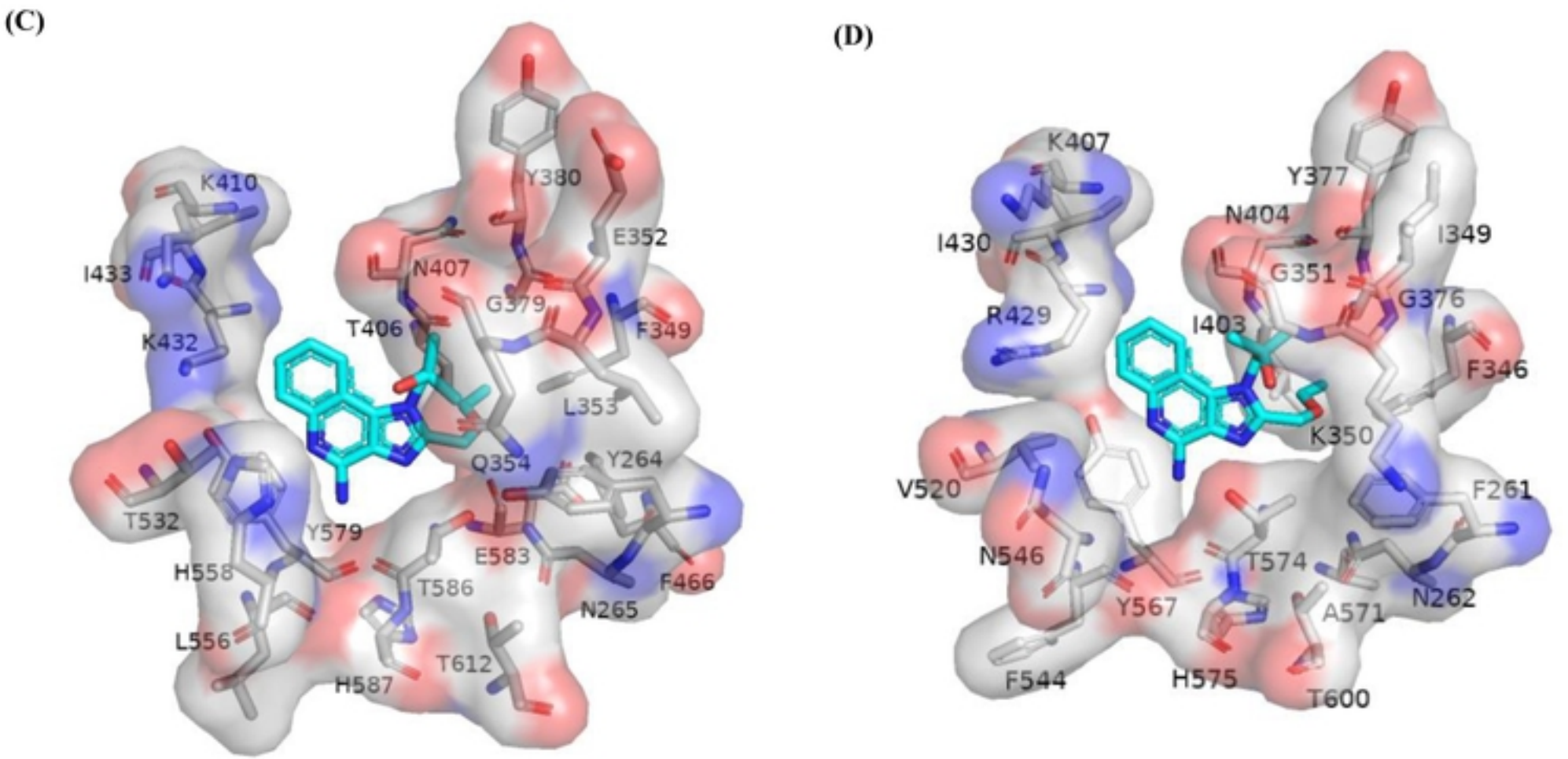

Fig8